Project Acronym	CORMORAN (ANR 11-INFR-010)
Document Title	D2.3 - Final Channel Measurement Campaign
Contractual Date of Delivery	M17 (31/05/2013)
Actual Date of Delivery	28/06/2013
Editor	Oudomsack Pierre Pasquero & Raffaele D'Errico (CEA)
Authors	Oudomsack Pierre Pasquero, Raffaele D'Errico (CEA), Bernard Uguen, Stéphane Avrillon, Meriem Mhedhbi (UR1), Paul Ferrand, Arturo Mauricio, Claire Goursaud, Jean-Marie Gorce, Jimenez Guizar (INSA)
Participants	CEA, UR1, INSA
Related Task(s)	T2
Related Sub-Task(s)	ST2.2
Security	Public
Nature	Technical Report
Version Number	1.0
Total Number of Pages	43

CONTACTS & CORRESPONDENCE

Oudomsack Pierre Pasquero (CEA)

- Address: CEA-Leti Minatec, 17 rue des Martyrs, Bât. 51D, p. D423, 38054 GRENOBLE, cedex 9, France
- Email: oudomsackpierre.pasquero@cea.fr
- Tel: (+33) (0)4 38 78 24 35

Raffaele D'Errico (CEA)

- Address: CEA-Leti Minatec, 17 rue des Martyrs, Bât. 51D, p. D423, 38054 GRENOBLE, cedex 9, France
- Email: raffaele.derrico@cea.fr
- Tel: (+33) (0)4 38 78 56 47

TABLE OF CONTENT

ABSTRACT

This document presents the *Wireless Body Area Network* (WBAN) channel measurement campaigns carried out in the frame of Task 2, and more exactly in the sub-task ST2.2. Since detailed narrow band and ultra-wide band (UWB) *On-body* channel models have already been provided in the D2.2 [1], no specific *On-Body* channel measurement campaign have been carried out. Thus, one of the measurement campaigns is totally focused on O*ff-body* radio links. Furthermore, one of the main contributions of the CORMORAN project being the development of novel cooperative communication schemes, a measurement campaign in a cooperative communication context has been performed. In this measurement campaign, *On-body*, O*ff-body* and *Body-to-Body* radio links have been measured simultaneously. Finally, in addition to these measurement campaigns, previous CEA and INSA *On-body* channel measurements in walking scenarios and previous UR1 human activity monitoring measurements are analysed in this deliverable.

As a main output of this deliverable, data channel measurements are now available for the sub-task ST2.3. Detailed analysis and channel models based on these measurements will be provided in the D2.4. Thus, the so-obtained channel models will feed the development of the physical simulator related to the sub-task ST2.4.

1. INTRODUCTION

A good understanding of channel characteristics is of fundamental importance in order to design operative and reliable communication systems. Physical (PHY), Medium Access Control (MAC) and Upper Layers protocols are strictly connected to the knowledge of propagation mechanisms and channel models.

In this manner, one of the tasks of the CORMORAN project is the modeling of WBAN channels in order to provide a physical simulator for the design of communication and localization systems. Some previous WBAN channel models developed at CEA-Leti were already provided in the D2.2 [1]. In this deliverable, we mainly present the final WBAN channel measurement campaigns which have been performed at CEA-Leti in the frame of Task T2. Thus, *Off-body* measurements and more general WBAN measurements in a cooperative communication context have been performed and are presented in section 2 and section 3 respectively. Some of the *Off-body* measurements have been processed using a modeling tool presented in the D2.2 and are analyzed in the sub-section 2.4.

In addition to these measurements, previous CEA and INSA *On-body* channel measurements in walking scenarios have been processed. Their analyses concerning the characterization of space-time correlation properties and asymmetry radio links are presented in section 4.

Furthermore, previous UR1 human activity monitoring channel measurements are presented and analyzed in section 5. The objective of this analysis is the identification ot the most important parameters related to human mobility.

2. OFF-BODY CHANNEL MEASUREMENTS

2.1. OVERVIEW

Off-Body channel measurements have been performed at CEA-Leti using a CTIA/IEEE standardized phantom. One of the objectives of these measurements is to characterize the angle of arrival (AoA) of the paths when receivers are located on a human subject. For that purpose, the *Space Alternating Generalized Expectation-maximization* (SAGE) algorithm developed and validated in D2.2 [1] has been used to process the measurements. The estimation of the AoA requires the exploitation of an antenna array at the receiver (Rx) side. In our measurements, a virtual antenna array was classically realized using a (X, Y) positioner available at CEA. Other off-body channel characteristics which will be investigated in the D2.4 will be the path loss and the power delay profile.

At the transmitter (Tx) side, an antenna was placed on a mast. And at the Rx side, three antennas were placed on the phantom. The measurements have been performed in two different rooms, for several distances d_{off} separating the Tx antenna to the phantom (from 1 m to 8 m with a step equal to 1 m), and for several phantom orientations Φ (from 0° to 180° or 315° with a step equal to 45°) as illustrated in Figure 1.

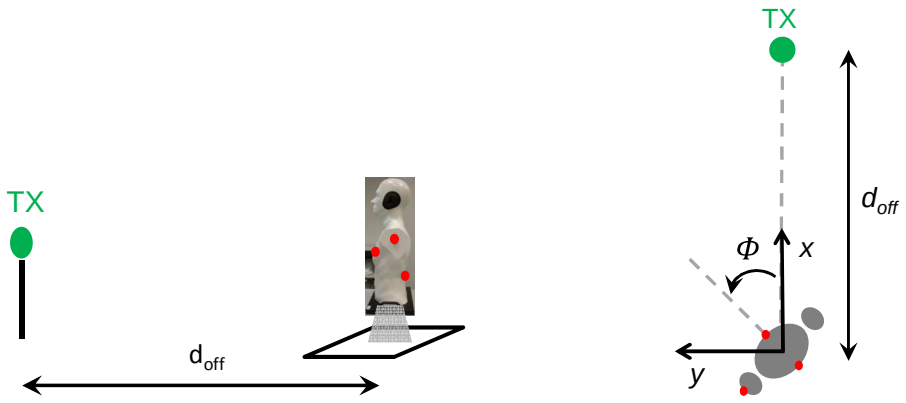

Figure 1 : Off-Body measurements illustration, side and top view

2.2. MEASUREMENT STEP-UP

A mechanical mount was necessary to place the phantom on the (X, Y) positioner. Thus, we realized a column in steel shown in Figure 2. The so-obtained mechanical mount allows a complete rotation of the phantom in azimuth with a step equal to 15°. The interest of this rotation is to analyze the influence of the body orientation according the transmitter.

Figure 2 : Pictures of the realized mechanical mount for the phantom placement on the (X, Y) positioner

The measurements have been performed using a Rohde & Schwartz ZVA24 4-ports Vector Network Analyzer (VNA) on an ultra-wide frequency band: [3 – 10] GHz, so-providing a good resolution for the estimation of the path delays. The frequency step was set at 8 MHz. The VNA characteristics allowed us to measure three different channel transfer functions (CTFs) simultaneously as illustrated in Figure 3. Therefore it was possible to choose three antenna locations on the phantom. According to the results of the user's questionnaire presented in D1.1 [2], we chose the torso, the back and the left shoulder of the phantom, as shown in Figure 4, which correspond to the three favorite locations for the *Coordinated Group Navigation* (CGN) applications.

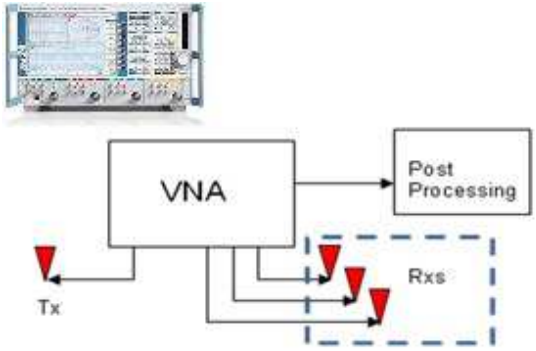

Figure 3 : Test bed with R&S ZVA24 vector Network Analyzer 4-ports

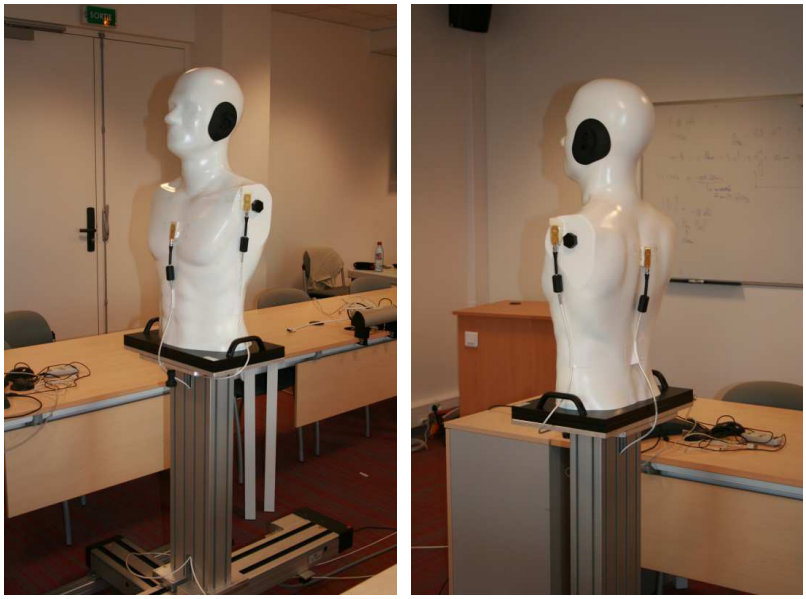

Figure 4 : Antenna locations on the phantom: torso, left shoulder and back

A Top Loaded Monopole (TLM) antenna, omnidirectional in azimuth, was used at the Tx side. Its radiation pattern in elevation for different frequency values is given in Figure 5. The Tx antenna was placed at the top of a mast at a height similar to that of the Rx antenna located on the torso of the phantom. At the Rx side, UWB dipole antennas [4] were used. They are omnidirectional in azimuth as shown in Figure 6. More details on the characteristics of these antennas are given in D2.1.

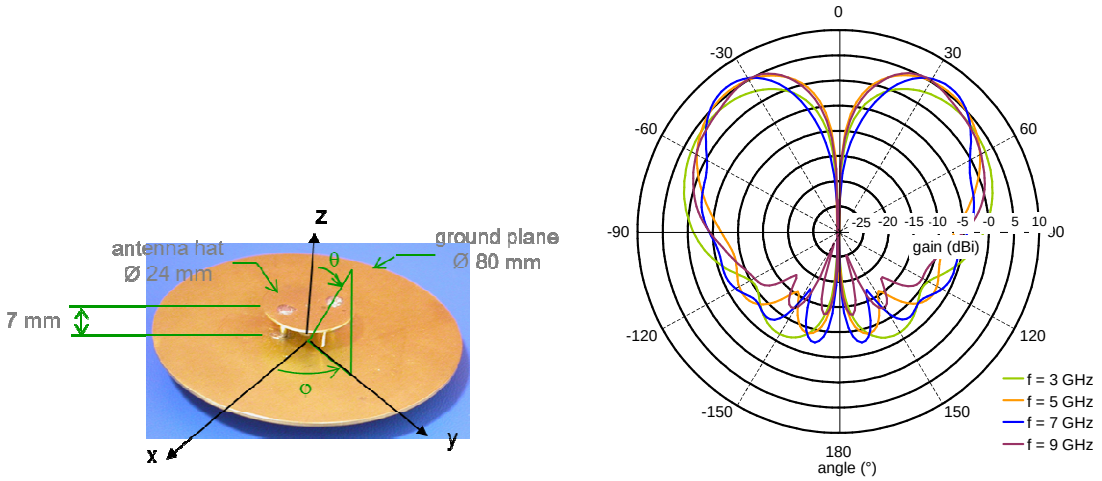

Figure 5 : Top Loaded Monopole antenna characteristics

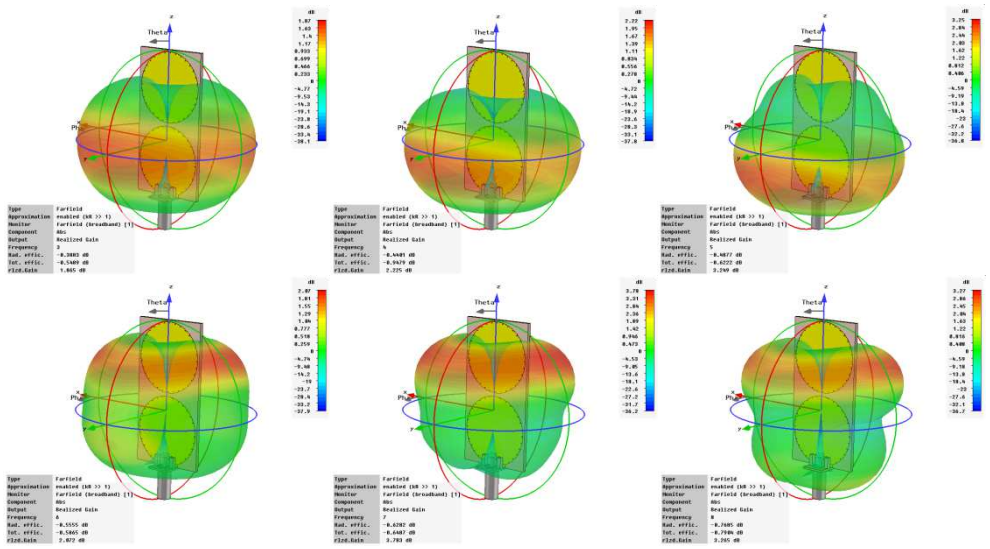

Figure 6 : UWB printed dipole gain pattern at different frequencies

The general objective of the Off-Body measurements being the analysis of the influence of the presence of a body, we performed benchmark measurements without phantom using one Rx antenna. Instead of the phantom, a little mast was placed on the (X, Y) positioner (Figure 7). The Rx antenna was so-placed at a similar position to that of the torso.

Figure 7 : Picture of the Rx antenna placed on a mast to perform the benchmark measurements

2.3. MODELING TOOL

As previously mentioned, an iterative high-resolution algorithm, namely *Space Alternating Generalized Expectation-maximization* (SAGE) [6] [7], developed and validated in D2.2 was used to process the measurements. Here, we remind the general principles of this algorithm.

2.3.1 OVERVIEW OF SAGE ALGORITHM

Based on the *Expectation Maximization* (EM) algorithm [8], SAGE algorithm has been proposed for the first time for channel parameters estimation by B. Fleury in [6]. In [9],

Chong *et al.* proposed a frequency-domain version of SAGE for Single-Input Multiple-Output (SIMO) system, which has been extended by Matthaiou *et al*, to Multiple-Input Multiple-Output (MIMO) systems [10]. UWB and spherical wave features have been introduced by Haneda *et al.* in [11] and [12]. Finally, S. Van Roy *et al.* adapted the UWB SAGE algorithm for BAN scenarios in [13].

The SAGE algorithm allows the estimation of the parameters of the multipath components (MPCs). In our case, we will focus on the estimation of the number of paths, their amplitudes, delays and angles of arrival (AoAs). Let us remind that the AoA estimation necessitates the use of an antenna array at Rx side. In our measurements, we defined 5 x 5 uniform rectangular antenna array. The inter-space antenna was equal to the half of the wavelength of the highest frequency.

Similarly to the EM method, the SAGE algorithm is characterized by an Expectation step (E-step) and a Maximization step (M-step). The M-step is based on maximum likelihood (ML) detectors. It consists in testing all the possible values of the parameters of each path and retaining the most likely. The E-step is an interference cancellation function. It consists in cancelling the contributions of the interfering MPCs from the measured channel transfer function (CTF) allowing a better estimation of the considered MPC parameters in the M-step.

SAGE algorithm can be implemented in the time domain or in the frequency domain. We chose to implement it in the frequency domain which is mathematically more suitable for UWB signals.

2.3.2 ALGORITHM DESCRIPTION

- *Channel Transfer Function expression*

First of all, let us express the channel transfer function (CTF) measured on the m-th antenna at the n-th frequency point of the considered bandwidth. It is equal to the sum of all the MPCs contributions:

$$H(m,n) = \sum_{l=1}^{L} \alpha_l(n) \underbrace{\exp(-j2\pi f_n \tau_l)}_{\text{phase rotation due to delay}} \underbrace{\exp\left(-j2\pi \frac{\langle e(\phi_l,\theta_l), r_m \rangle}{\lambda_n}\right)}_{\text{phase rotation due to antenna position and AoA}} \underbrace{D(n,\phi_l,\theta_l)}_{\text{=1 if isotropic antenna}} + W(m,n) \quad \textbf{(1)}$$

- l and L are the MPC index and the total number of MPCs respectively
- α_l is the amplitude
- τ_l is the delay
- ϕ_l and θ_l are the angles of arrival (AoA) in azimuth and in elevation respectively
- $e(\phi_l, \theta_l)$ is a unitary vector whose direction is that of the l-th path

- r_m is the coordinates vector of the m-th antenna
- λ_n is the wavelength for the frequency f_n
- $D(n, \phi_l, \theta_l)$ is the product of Tx and Rx complex antenna gains depending of the frequency f_n and the angles of arrival
- W(m,n) is an additive white Gaussian noise sample.

- *E-step*

The E-step allows estimating the signal contribution of the l-th MPC by subtracting the other MPC contributions from the measured CTF as:

$$\widehat{\boldsymbol{X}}_l = \boldsymbol{H} - \sum_{\substack{l'=1 \\ l' \neq l}}^{L} \widehat{\boldsymbol{X}}_{l'}(\widehat{\boldsymbol{\psi}}_{l'}) \quad (2)$$

where $\widehat{\boldsymbol{X}}_l$ is the estimated contribution of the l-th MPC and $\widehat{\boldsymbol{\psi}}_l$ represents the estimated parameters of the l-th MPC. This operation is performed by a parallel interference cancellation (PIC). However, it has been shown in [9] that in a rich multipath environment, a successive interference cancellation (SIC) has a better performance. In this scheme, the MPCs are ordered according to their received powers and the MPCs are estimated and cancelled successively from CTF. Thus, only the MPCs whose power is higher than that of the considered MPC are cancelled from the CTF.

$$\widehat{\boldsymbol{X}}_l = \boldsymbol{H} - \sum_{l'=1}^{l-1} \widehat{\boldsymbol{X}}_{l'}(\widehat{\boldsymbol{\psi}}_{l'}) \quad (3)$$

- *M-step*

It is then possible to estimate the l-th MPC parameters using ML detectors, corresponding to the M-step. For this purpose, a correlation function is defined as:

$$z_l(\tau, \phi, \theta\,;\, \widehat{\boldsymbol{X}}_l) = \sum_{n=1}^{N} \sum_{m=1}^{M} \exp(+j2\pi\, f_n\, \tau)\ \exp\left(+j2\pi \frac{\langle e(\phi, \theta), r_m \rangle}{\lambda_n}\right) \times \hat{X}_l(m,n) \quad (4)$$

The M-step consists in testing all the possible τ, ϕ and θ values and retaining those which maximize the absolute value of the correlation function. In order to limit the complexity of this step, the parameters of each MPC are not estimated in parallel but successively. Classically, the first parameter to be estimated is the delay. For this purpose, the angles of arrival values estimated during the previous iteration are used in the correlation function as

shown in equation **Erreur ! Source du renvoi introuvable.**). Then, the angles of arrival are estimated taking into account the updated estimated delay.

$$\begin{aligned}
\hat{\tau}_l^{(i)} &= \arg\max_{\tau} \left| z_l\left(\tau, \hat{\phi}_l^{(i-1)}, \hat{\theta}_l^{(i-1)}; \hat{\boldsymbol{X}}_l\right) \right|^2 \\
\hat{\phi}_l^{(i)} &= \arg\max_{\phi} \left| z_l\left(\hat{\tau}_l^{(i)}, \phi, \hat{\theta}_l^{(i-1)}; \hat{\boldsymbol{X}}_l\right) \right|^2 \\
\hat{\theta}_l^{(i)} &= \arg\max_{\theta} \left| z_l\left(\hat{\tau}_l^{(i)}, \hat{\phi}_l^{(i)}, \theta; \hat{\boldsymbol{X}}_l\right) \right|^2
\end{aligned} \tag{5}$$

Once the delay and the angles of arrival of a MPC are estimated, the amplitude is simply computed by the following equation:

$$\hat{\alpha}_l = \frac{1}{M} z_l\left(\hat{\tau}_l^{(i)}, \hat{\phi}_l^{(i)}, \hat{\theta}_l^{(i)}; \hat{\boldsymbol{X}}_l\right) \tag{6}$$

Let us note that here, one average amplitude is estimated by MPC for all the bandwidth. In the case of an UWB channel, the amplitude can vary in the frequency domain. More particularly, the phase of the Tx and Rx antenna gains, which are included in this amplitude, can vary significantly. To limit this inconvenient, Haneda and Takada proposed in [11] to divide the considered frequency band in sub-bands. Hence, the M-step is performed in all the sub-bands in parallel. Thus, one estimated average amplitude is computed by sub-band by MPC. This method allows a better estimation of the MPC amplitude. However, it reduces the time resolution of the algorithm since it becomes function of the inverse of the sub-band width. In other words, the delay estimator performance decreases.

- *Initialization cycle*

At the start of the algorithm, no estimation of the MPC parameters is available. Therefore, no interference cancellation can be carried out for the estimation parameters of the first MPC and no estimated value of the angles of arrival is available for delay estimation of the MPCs. In [7], B. Fleury proposed an initialization cycle (i=0) in which a SIC is exploited for E-step and the correlation function is modified for M-step. More precisely, delay estimation is performed without taking into account the effects of the angles of arrival in the initialization cycle. The initialization allows providing not only initial estimations of the MPC parameters but also, an estimation of the total number of MPCs. For this purpose, SIC and M-step are performed successively until the estimated power of a MPC is not significant.

Different criterion can be used to determine if an estimated MPC is significant or not. It can be the comparison with the power of the strongest path or the noise power. A classical criterion used is the comparison of the regenerating CTF power (corresponding to the estimated interference in the E-step) with that of the measured CTF. For instance, if the regenerated CTF power is higher than 90% of the measured CTF power, it could be considered that the estimation of other MPCs parameters is not necessary. Unfortunately, it has been observed that the high-resolution algorithms do not completely capture all of the power from the measured impulse responses. The difference between the measured impulse responses and the reconstructed ones is usually referred to as the diffuse multipath components (DMC) [14] [15]. In the SAGE version we implemented, the criterion we use is the comparison between the noise power and the estimated path power. More precisely, we consider that a path is not significant if its estimated power is not at least 10 dB higher than the measured noise power. Figure 8 summarizes in a flow chart the initialization cycle principle of SAGE algorithm.

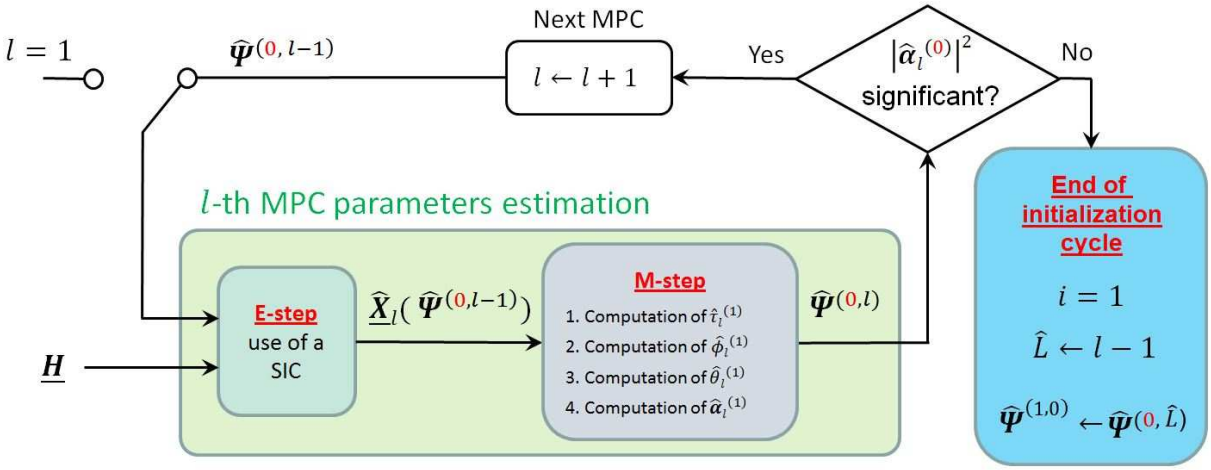

Figure 8: Flow chart of SAGE algorithm during the initialization cycle

2.4. PRELIMINARY ANALYSIS

Off-Body channel measurements have been processed using SAGE algorithm developed at CEA-Leti. Let us note that the signal frequency band was divided in sub-bands of 1 GHz in SAGE processing. In the sequel, we present the results obtained for a distance d_{off} = 8m and for 4 phantom orientations (0°, 90°, 180° and 270°).

2.4.1 ANTENNA LOCATION INFLUENCES

Here, we analyze the influence of the presence of the phantom and that of the antenna location on the phantom. Figure 9 gives the MPC parameter values estimated without and with phantom for an orientation Φ = 0°.

Each point corresponds to one detected path. The points are plotted in polar coordinates. The angle represents the estimated AoA in azimuth. The distance separating the points to the

center of the circle represents the estimated time delays multiplied by the speed of the light in free space, i.e. the distances traveled by the paths in meter. Finally, the colors of the points represent the estimated path powers in dB. Let us note that we do not represent the estimated AoAs in elevation. Indeed, since the virtual antenna array used at the Rx side was in 2 dimensions, the resolution of the AoA in elevation is very weak. In addition to representing the estimated MPC parameters, we give the estimated number of significant paths and the relative SAGE regenerated channel power in %. Similarly to [15], SAGE roughly estimates 2/3 of the measured channel power.

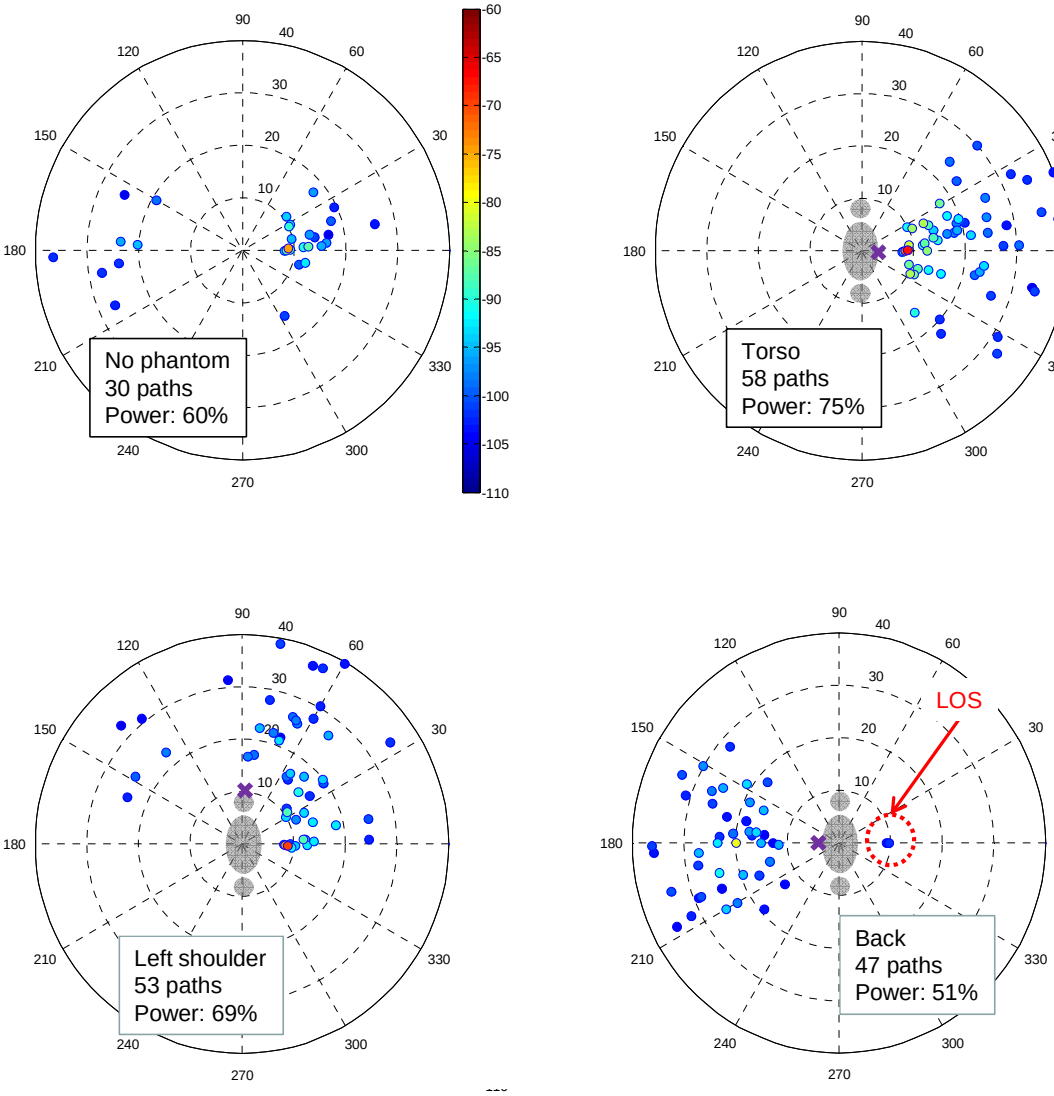

Figure 9 : SAGE estimated MPC parameters without phantom, on the torso, left shoulder and the back - phantom orientation $\Phi = 0°$ - $d_{off} = 8m$

The first noticeable observation is that more MPCs are detected by SAGE with presence of the phantom. For instance, in the case the Rx antenna is located on the torso, paths coming from the front of the phantom only are detected, including the path in line-of-sight (LOS). Without presence of the phantom, paths coming from the front are also detected but much less.
A similar observation is also noticeable in the case the Rx antenna is located on the back. Without presence of the phantom, some paths coming from the backside are detected, which certainly result from reflections on the bottom of the room. With presence of the phantom, much more paths coming from the backside are detected. Furthermore, some of them are more powerful than those detected in the case without phantom.

For a better understanding of these observations, we plot in Figure 10 channel impulse responses (CIRs) with and without presence of the phantom for an orientation $\boldsymbol{\Phi}$ = 0°. In the case the Rx antenna is located on the torso, it clearly appears that the measured CIR energy is stronger with than without presence of the phantom. Furthermore, the strongest paths are twice more powerful in presence of the phantom. Similar observations are visible in the case the Rx antenna is located on the back. Obviously, due to the obstruction generated by the phantom, the first part of the CIR is more powerful without phantom. For time delays higher than 60 ns, the measured CIR energy is much more powerful with than without phantom.
As demonstrated in D2.1 [3], the vicinity of the body generates a modification of the radiation pattern of the antennas which could make the antennas more directives. This could explain the fact that some detected paths are more powerful in presence of the phantom. Furthermore, a better directivity of the antennas can amplify the power of some paths which were lower than the noise power without presence of the phantom.

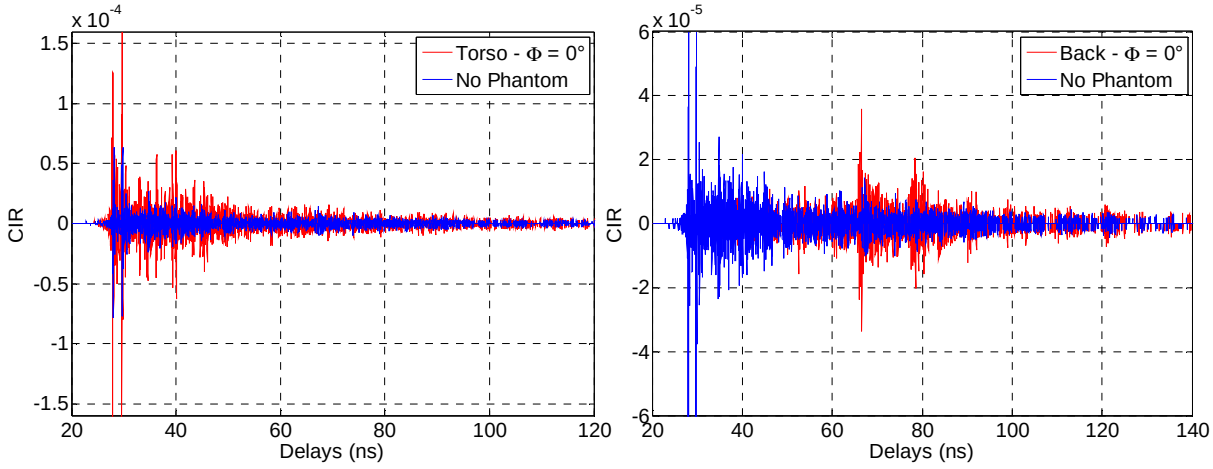

Figure 10 : Measured Channel Impulse Responses with and without presence of the phantom, Rx antenna on the torso and the back, d_{off} = 8m, phantom orientation $\boldsymbol{\Phi}$ = 0°

2.4.2 BODY ORIENTATION INFLUENCES

In order to evaluate the influences of the phantom orientation, we give in Figure 11, Figure 12 and Figure 13 the estimated MPCs for d_{off} = 8m and 4 phantom orientations in the case the Rx antenna is located on the torso, the left shoulder and the back respectively.

Logically, we observe that the vast majority of the detected paths come from the side the antenna is located on the phantom whatever the phantom orientation. In a few cases, for instance, the case the Rx antenna is located on the back and the phantom orientation $\Phi = 0°$, we observe one or two paths coming from the opposite side of the phantom with an estimated azimuthal AoA equal or close to 0°. They could correspond to creeping waves around the torso. Besides the estimated distances traveled by these paths are a little larger than d_{off}. This little difference of distance could correspond to the distance traveled by the waves around the torso of the phantom.
Other interesting observations are the visible symmetries between graphics of different figures. For instance, the graphic corresponding to the case the Rx antenna is located on the torso with a phantom orientation $\Phi = 180°$ is very similar to that corresponding to the case the Rx antenna is located on the back with a phantom orientation $\Phi = 0°$.

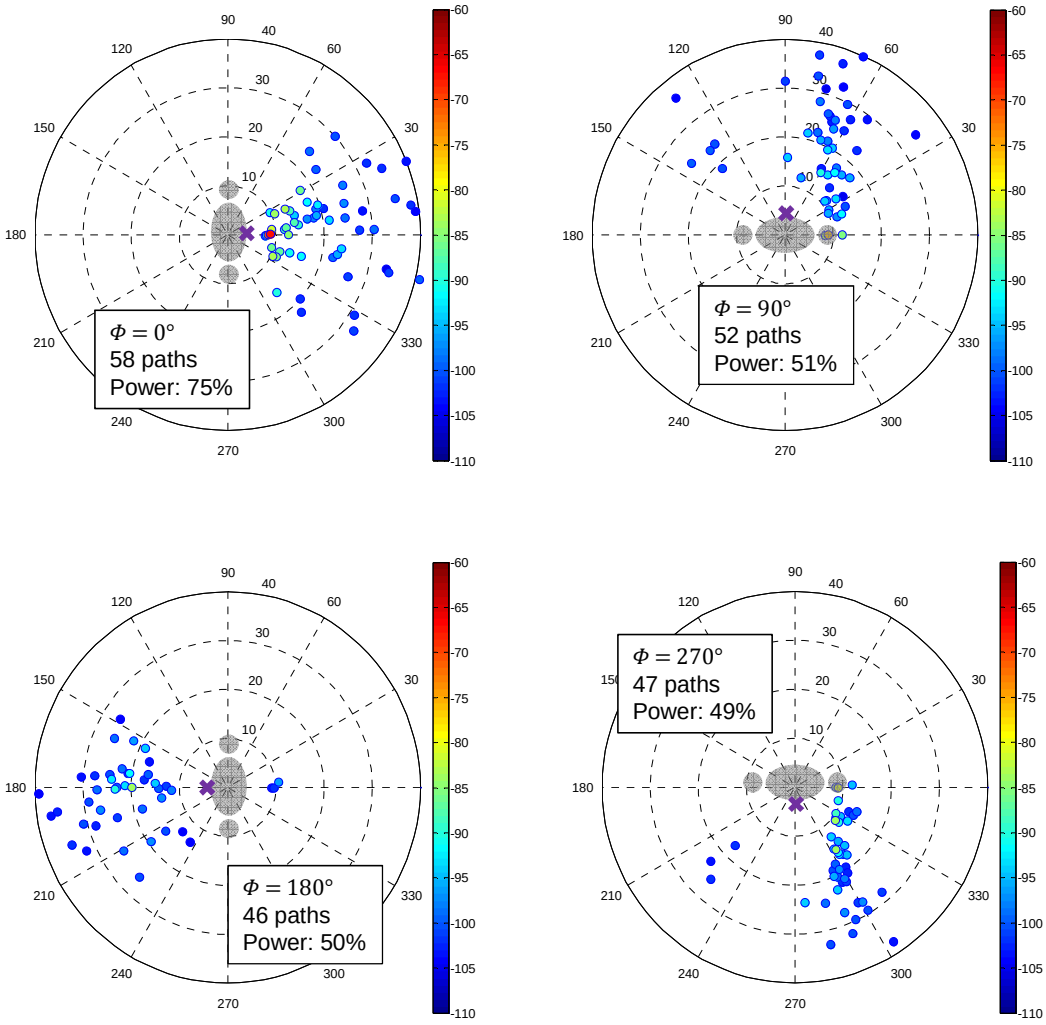

Figure 11 : SAGE estimated MPC parameters with phantom – Rx antenna on the Torso - d_{off} = 8m

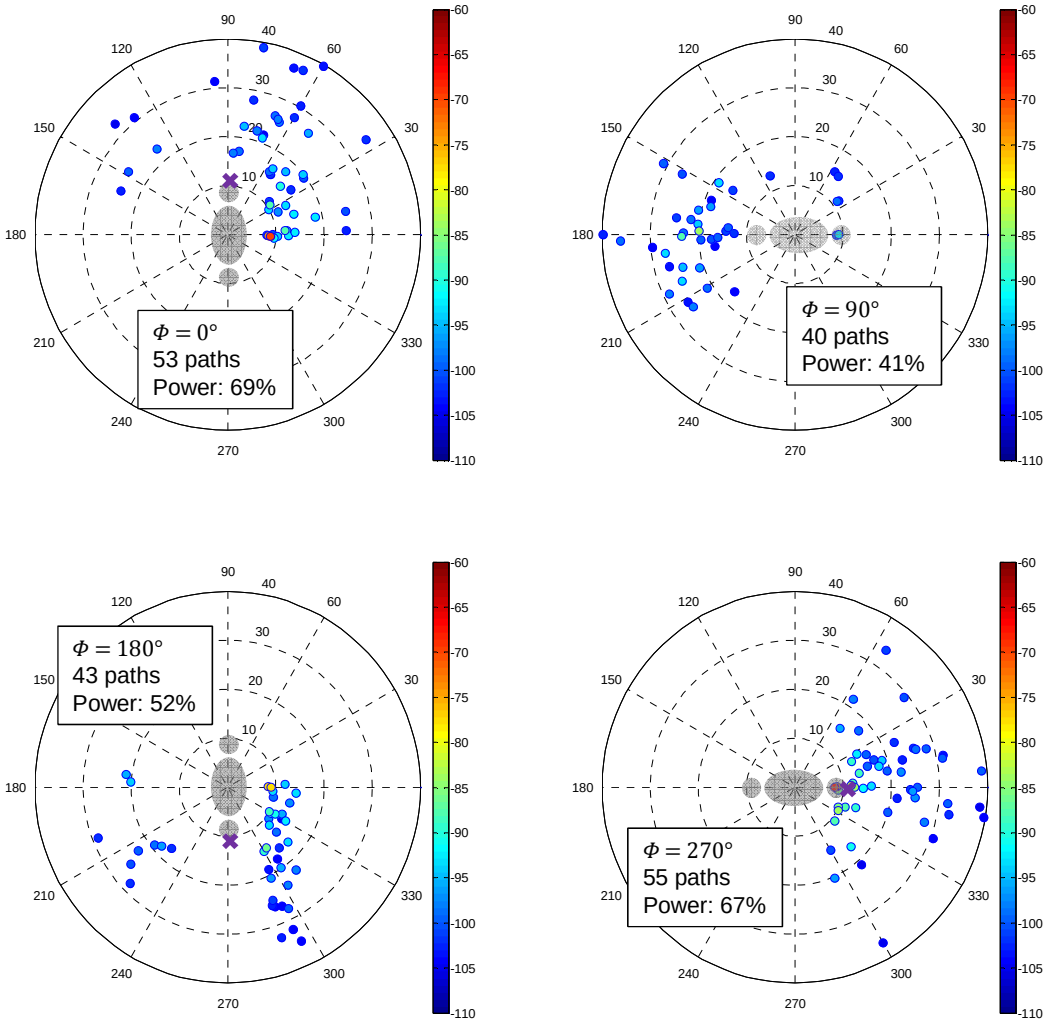

Figure 12 : SAGE estimated MPC parameters with phantom – Rx antenna on the Left Shoulder - d_{off} = 8m

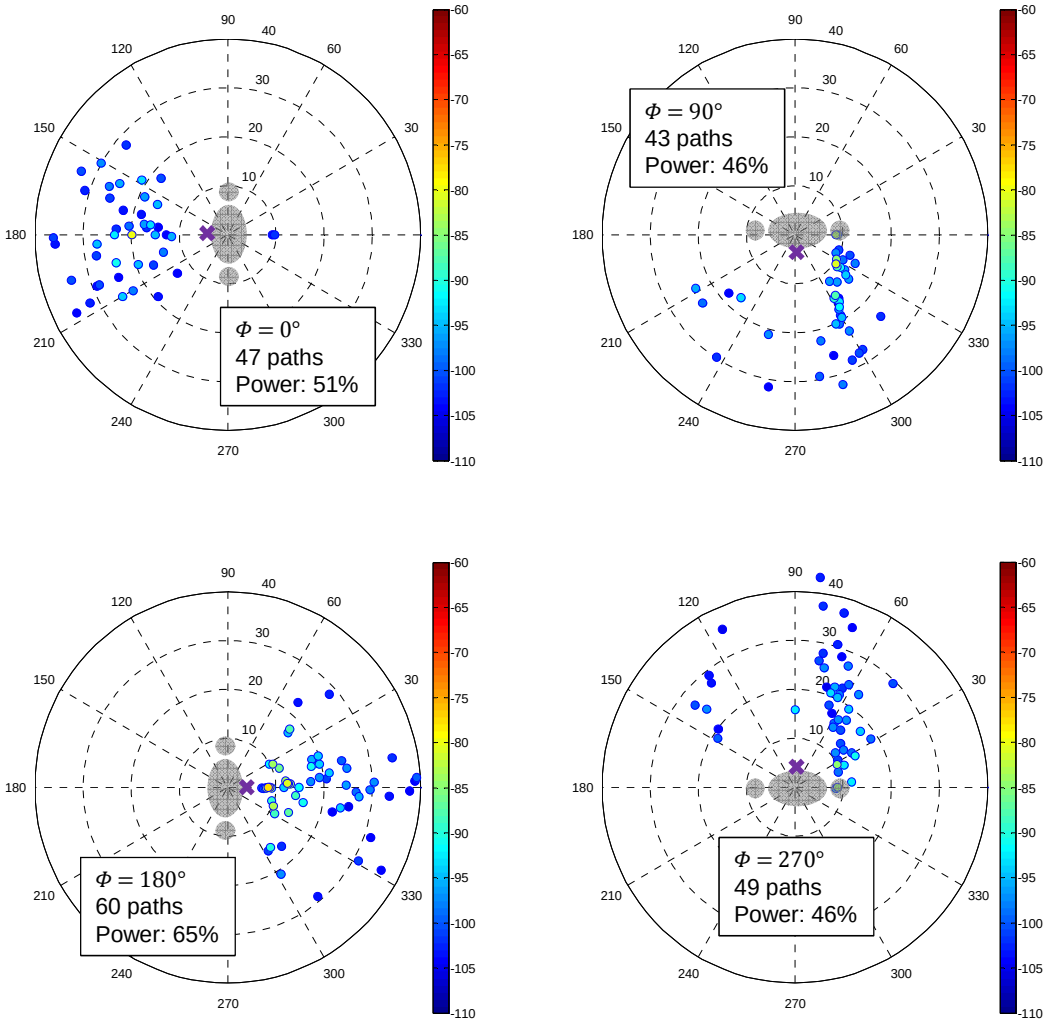

Figure 13 : SAGE estimated MPC parameters with phantom – Rx antenna on the Back - d_{off} = 8m

2.5. OUTPUTS FOR THE PROJECT

These Off-Body channel measurements will be analyzed more in detail in the sub-task 2.3. More precisely, an AoA modeling in azimuth should be proposed. The results will be compared with the deterministic model which will be proposed by UR1. Ideally, the analysis of these measurements should validate the UR1 deterministic model. Possibly, a statistical model based on these measurements could be injected in the general Off-Body channel model and combined with deterministic models.

The complete analysis of these measurements will also be useful for the sub-task 3.2 concerning the development of novel algorithms for new cooperative location and tracking functions. Indeed, the analysis of these measurements will provide a better knowledge on the time delay of the most powerful path.

3. BAN MEASUREMENTS IN A COOPERATIVE CONTEXT

3.1. MEASUREMENT SET-UP

BAN measurements have been performed at CEA-Leti in cooperative communication contexts in the sense that On/Off-Body and Body-to-Body channels were measured simultaneously. For that purpose, we used the phantom, an external node (a mast with an antenna at its top) and human subjects. In total, two human subjects have been involved in this measurement campaign which has been carried out in an indoor environment.

For each measurement acquisition, one human subject, the phantom and the external antenna were aligned. The human subject was always located between the external node and the phantom. The antennas carried by the human subjects and the phantom were Thomson UWB dipoles. That used for the external gateway was a TLM. Two antennas were located on the human subject, one on the torso and the other one on the back. One antenna was located on the torso of the phantom. For convenience, we number the so-obtained nodes from 1 to 4 as illustrated in Figure 14. Strictly all the radio links (On/Off/Body-to-body) were simultaneously measured by a VNA whatever the mobility scenario was.

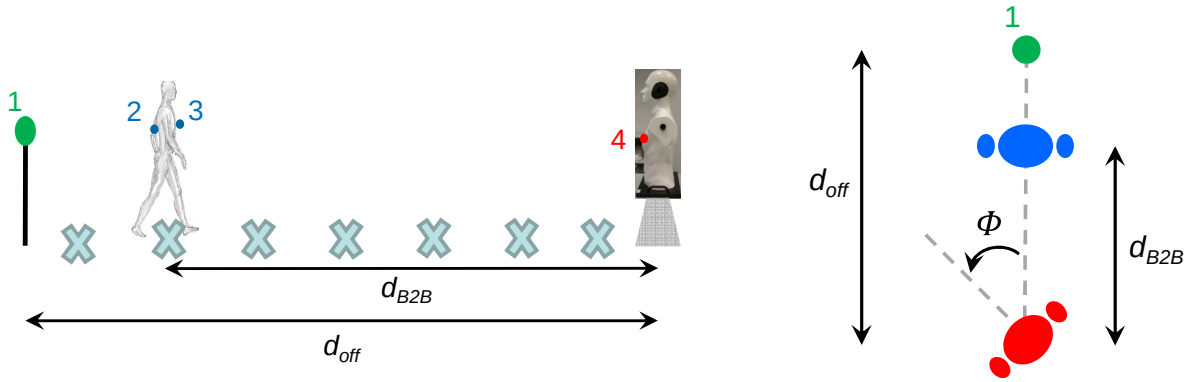

Figure 14 : Static UWB measurement campaign illustration in a cooperative scenario – Side view and Top view

Static measurements, i.e. the human subject did not move, have been performed on an ultra-wide frequency band [3 – 10] GHz. According to the maximum inter-body distances defined in D1.1, the distance d_{B2B} separating the human subject and the phantom varied from 1m to 7m, with a step equal to 1m. The off-body distance d_{off} between the external gateway to the phantom was set to 8m. For each location of the human subject, measurements were performed for 8 phantom orientations Φ varying from 0° to 315° with a step equal to 45°.

Figure 15 : Picture of a static UWB measurement in a cooperative scenario

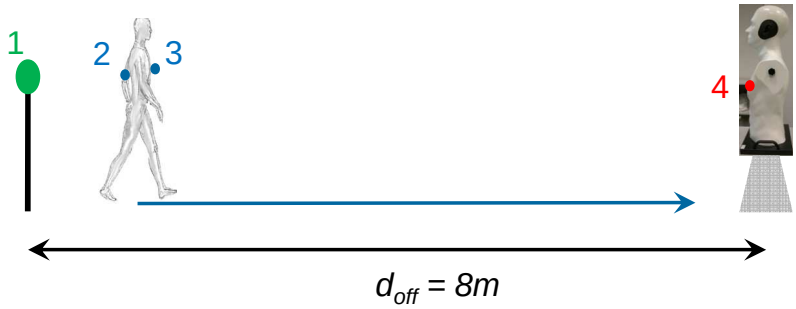

Figure 16 : Dynamic measurement campaign illustration in a cooperative scenario

Dynamic measurements, i.e. the human subject walked, have also been performed. Due to the frequency sweep duration of the VNA, it was not possible to possible to perform measurements on a wide frequency band. Thus, the measurements have been performed at 4 GHz which corresponds to the center frequency of the UWB lower band. The analysis of these measurements at 4 GHz, which will be presented in D2.4, will be extendable to the entire UWB lower band. Indeed, in the next section, we show that the analysis and observations made at 2.4 GHz are the same at 4.2 GHz.

The dynamic measurements have been carried out for 5 phantom orientations: from 0° to 180° with a step equal to 45°. For each phantom orientation, 5 measurement acquisitions corresponding to 5 walk cycles were performed by human subject. All the walk cycles corresponded to the same straight line trajectory. The departure of the trajectory corresponded to the case d_{B2B} = 7m, and the arrival to d_{B2B} = 1m. Therefore, one cycle of walk corresponded to a walk of 6m.

3.2. FUTURE ANALYSIS

Similarly to the state-of-the-art presented in D2.2 on the characterization and modeling of Off-Body and Body-to-Body channels in static scenarios, a characterization of the UWB path loss will be carried out in D2.4. More precisely, a UWB path model will be proposed in function of the distances and the phantom orientation for the static scenarios. Furthermore, an analysis will be carried out on the power delay profile (PDP), i.e. the number of paths and the delay dispersion, as it has been done for On-Body channel in [17]. Concerning the dynamic scenarios, space-time correlation properties will be analyzed between all the kinds of radio link (On/Off/Body-to-Body).

3.3. OUTPUTS FOR THE PROJECT

Correlation between the links can have a strong impact on the performance of cooperative techniques in communication, and can lead to overestimation or underestimation of the performances of the system [20]. The correlation encountered in WBAN is also very specific when compared to other communication problems, as it is scenario-based and strongly dependent on the body movements and positions [17] [21]. The input of this task for the whole project is thus two-fold; modeling the space-time correlation properties of On/Off/Body-to-Body links will allow a better design of the cooperative communication systems which will be proposed in the task 3, and the measurements will give a basis for simulation onto which the performance of protocols developed for higher layers may be evaluated. As of now, information about the link correlation is expected to be used by our team in the task 3 to select better relay partners.

4. PREVIOUS ON-BODY CHANNEL MEASUREMENT ANALYSIS

In addition to performing new measurement campaigns in novel scenarios, some previous On-Body measurements carried out at CEA-Leti and INSA have been processed and analyzed. CEA measurements had already been exploited for the On-Body channel characterization at 2.45 GHz [1]. Here, we focus on the signal measured at 4.2 GHz, the center frequency of the UWB lower band. In the sequel, we describe these measurement campaigns and analyze some space-time correlation properties.

4.1. MEASUREMENTS SET-UP

4.1.1 CEA MEASUREMENTS

The CEA measurement test bed was mainly composed by a pulse step generator and a power amplifier at the Tx side, whereas low-noise amplifiers were connected to a wideband real-time digital oscilloscope at the Rxs side, in a sort of SIMO configuration, as illustrated in Figure 17. The idea was to collect simultaneously up to four channel impulse responses (CIRs), each one corresponding to a different location on body. RF cables and antennas were obviously part of the test-bed.

The node emplacement considered for the measurement campaign performed is presented in Figure 18. In the sequel, we will focus only on the two links: Tx on heart and Rxs on left and right hand.

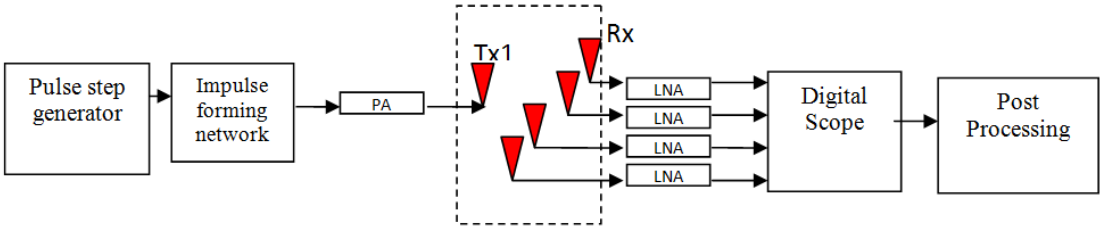

Figure 17 : Time domain channel measurement test-bed

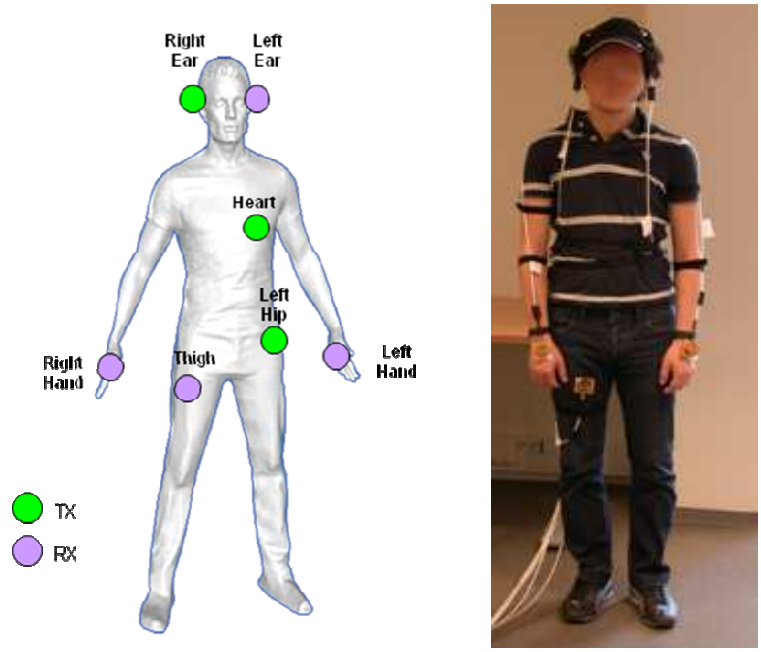

Figure 18 : Node emplacement for CEA On-Body measurements

Three human subjects have been involved in this measurement campaign for different mobility scenarios. Here, we will focus in the walking scenarios only. Each subject walked in regular way on a straight line of 3 meters in one direction then the opposite one. Finally, two walk cycles, and so two measurement acquisitions of 3 s, have been performed by each subject.

4.1.2 INSA MEASUREMENTS

When considering cooperation in BANs, a related measurement campaign has been conducted at INSA and aimed at sampling the quality of every link in a BAN in a quasi-simultaneous manner. The scenario considered a BAN composed of 6 nodes, located on the body as illustrated on Figure 19. The campaign focused on outdoor walking scenarios at 2.45 GHz, in a low interference and open environment.

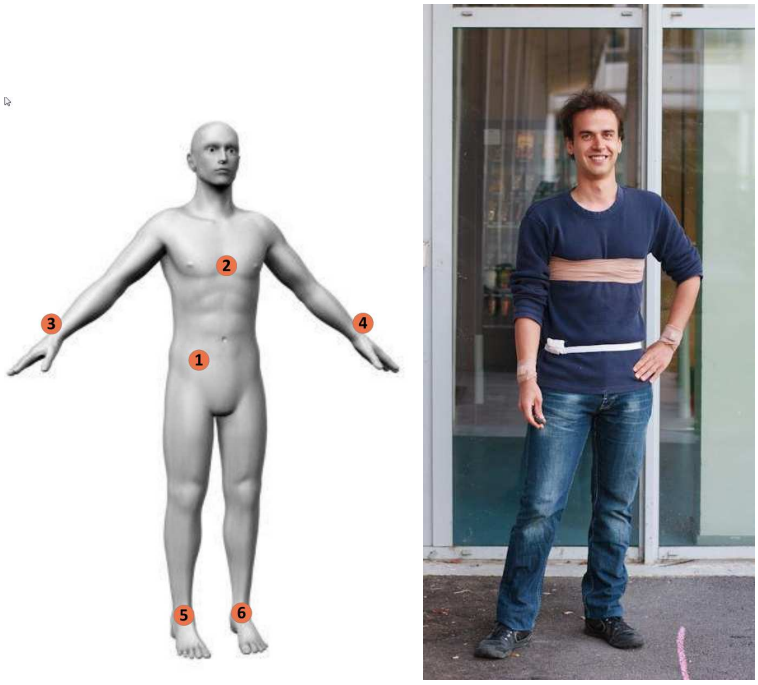

Figure 19 : Node position for the INSA On-Body measurements

The platform uses commercial sensors developed and marketed by HiKoB (www.hikob.fr) , a local startup on the INSA campus. The sensors embed a 32 bits ARM Cortex M3 processor and an Atmal AT86RF231 radio chipset, for which the physical layer is IEEE 802.15.4 compliant in the 2.4 GHz ISM band. As these sensors run on batteries and are equipped with a SD card-based storage, the platform is easy to deploy in any mobile indoor and outdoor scenario.

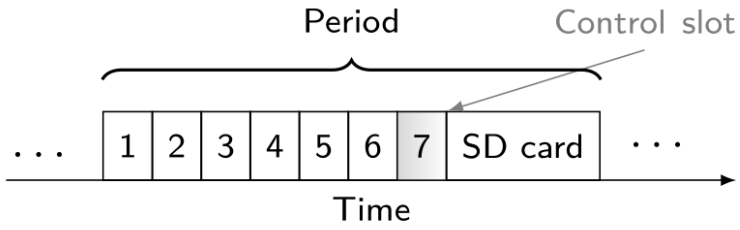

Figure 20 : Protocol used for the INSA measurement campaign

This mobility comes at the price of measurement accuracy, as the values sampled by the nodes are based on the received signal strength of the sensors and translated into an "Energy

Detection" (ED) metric whose relative error is +/- 1dB. The measurement protocol is shown on Figure 20. During a complete measurement period, the sensors transmit in turn and allow every other sensor in the network to sample the ED value. A handheld, seventh sensor has then a small window to mark the start and end time of the measurement. All sensors write the values they stored in memory for this sample on the SD-card at the end of the period.

4.2. SPACE-TIME CORRELATION

In the D2.2 and in [1], some space-time correlation properties between different On-Body radio links have been characterized at 2.45 GHz in walking scenarios. Here, we verify if some of these correlation properties still valid at 4.2 GHz, which is the center frequency of the UWB lower band. More precisely, we focus on the radio links for which Tx is on the heart and the Rxs are on the left and right hand [16].

4.2.1 SLOW FADING EXTRACTION

It is well known that in the power transfer function, one can distinguish slow and fast fading components as outlined by:

$$P(t) = G_0 \,.\, S(t) \,.\, F(t) \tag{7}$$

where G_0 represents the mean channel gain, S(t) and F(t) respectively the normalized slow and fast fading components [17].

In the sequel, we extract the normalized slow fading component from the measurements by applying a low pass filter. The filtering is practically realized by averaging the time-dependent power transfer function on a sliding time window which duration Δt is equal to 320 ms. The low pass filtering process is mathematically described by the following equation:

$$S(t) = \frac{1}{\Delta t} \int_{t-\Delta t/2}^{t+\Delta t/2} \frac{P(t)}{G_0} \tag{8}$$

Figure 21 shows an example of measured power transfer function and the corresponding extracted slow fading (without normalization) for two radio links: Tx on heart and Rxs on right and left hands in a walking scenario.

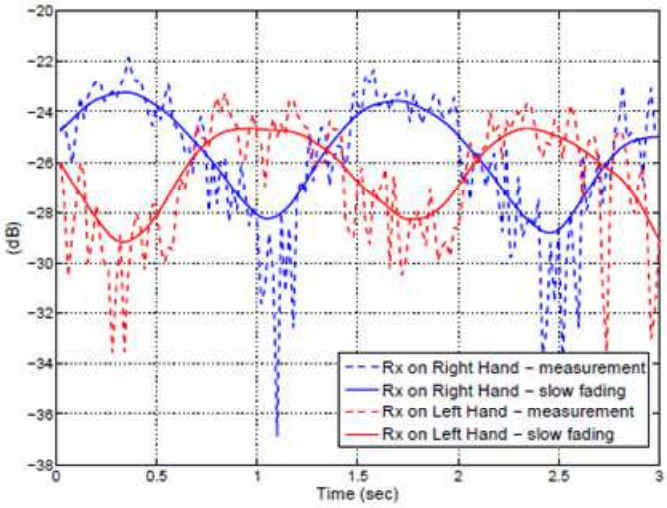

Figure 21 : Example of slow fading extractions (without normalization) – Tx on Heart – Δt = 320 ms

In WBAN communication systems, the slow fading, also known as shadowing, is mainly due to the movement of the human body that dynamically shadows the communication while moving. It has been shown in [17] and [18] that this effect is particularly evident when one of the antennas is placed on a limb, which is the case here. Furthermore, due to the geometry of the body, some interesting correlation properties can be observed in walking scenarios. For instance, Figure 21 clearly shows an opposite behavior, i.e. an anti-correlation property, between the two radio links.

4.2.2 CORRELATION METRIC

To quantify the correlation between on-body links, we define the following correlation metric:

$$\rho_{i,j}\left(t;T_{\text{obs}}\right)=\frac{\mathbb{E}\left[\left(S_{\text{TX},i}-\mathbb{E}\left[S_{\text{TX},i}\right]\right)\left(S_{\text{TX},j}-\mathbb{E}\left[S_{\text{TX},j}\right]\right)\right]}{\sqrt{\mathbb{E}\left[S_{\text{TX},i}^{2}-\mathbb{E}^{2}\left[S_{\text{TX},i}\right]\right]\mathbb{E}\left[S_{\text{TX},j}^{2}-\mathbb{E}^{2}\left[S_{\text{TX},j}\right]\right]}} \quad \textbf{(9)}$$

where E[.] represents the expectation operator and $S_{TX,\,i}$ the slow fading component in dB of the radio link associated to the Tx transmitting antenna position and the i-th receiving antenna position measured during the interval time [t - $T_{obs}/2$; t + $T_{obs}/2$]. Finally, $\rho_{i,j}$ represents the correlation value measured between two radio links on a time window which width is equal to T_{obs}.

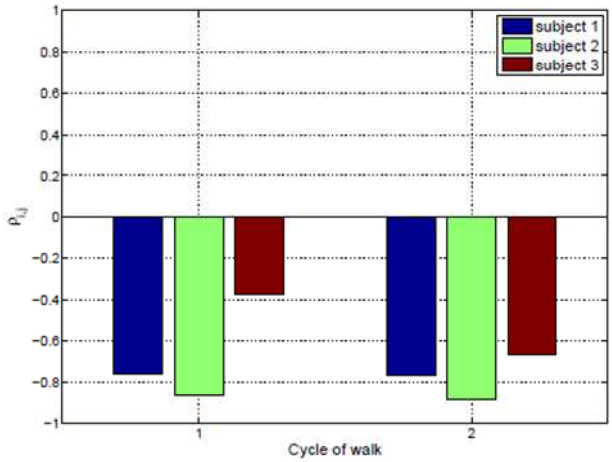

Figure 22 : $\rho_{i,j}$ measured for the three human subjects for both walk cycle - T_{obs} = 3s

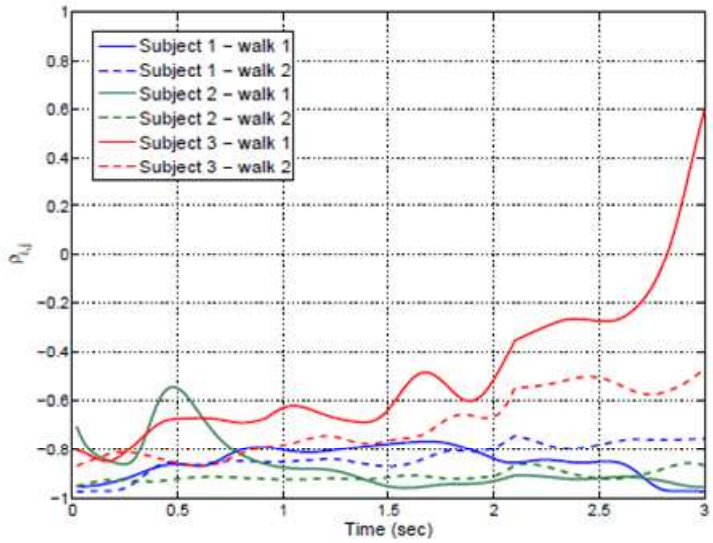

Figure 23 : $\rho_{i,j}$ measured for the three human subjects for both walk cycle using a sliding window - T_{obs} = 3s

4.2.3 MEASUREMENT ANALYSIS

From the correlation metric defined in (9), we analyze the correlation properties between the slow fading components of the two On-Body radio links: Tx on heart and Rxs on right and left hands, according to different widths of the observation time window T_{obs}. Note that in the sequel, we consider that the radio links are highly correlated (resp. anti-correlated) when the correlation metric is higher than 0.4 (resp. lower than -0.4).

Figure 22 gives the space-time correlation values measured for the three human subjects, for each walk cycle, for T_{obs} = 3s, i.e. T_{obs} equal to the duration of a walk cycle. It clearly appears that the two radio links are highly anti-correlated. This is what had been concluded in the state-of-the-art in D2.2 and in [1] at 2.4 GHz. Furthermore, for *subject* 1 and *subject* 2, the

correlation value does not vary significantly between the two walk cycles. Different correlation values are measured for *subject* 3 for the two walk cycles.

To analyze more in detail the space-time correlation properties of the On-Body measurements, we give in Figure 23 the correlation value in function of the time, using a sliding window which width is equal to T_{obs} = 1.8s. it clearly appears that the correlation characteristics are stationary in time. In the *walk cycle* 1 of *subject* 3, the increase of $\rho_{i,j}$ value during the last second is due to the fact that the subject prematurely finished his walk. It explains why the value difference measured for the two walk cycles of *subject* 3 in Figure 22.

4.3. LINK SYMMETRY

While the original goal of the measurement campaign was to assess the spatial correlation of the link qualities in a WBAN, the complete mesh allows the evaluation of the link symmetry and reciprocity. As seen on Figure 24, the quality of direct and reverse paths agree well enough, but a relative offset is apparent, especially on the 1—4 link where the reverse path is about 1 dB higher than the direct one.

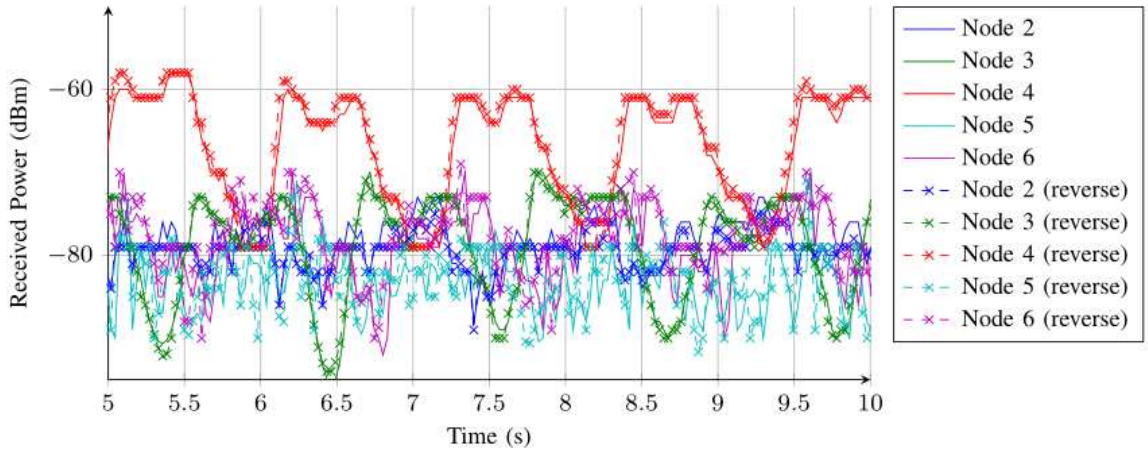

Figure 24 : Zoom on the link quality measured by node 1 (Hip) during a walking experiment

We conjectured that this offset was due, in part, to the varying *hardware* characteristics of the nodes. In particular, the transmission power is set through software, but is subjected to an uncertainty of +/- 3dB as indicated by the data sheet of the radio chipset. The sensitivity of the receiving hardware may also be causing these offsets.

We designed an experiment to assess if the symmetry offset was statistically significant, whether it was stable in time and dependent on the sensor hardware. Thus, we evaluated the mean difference of the link qualities as measured by each node over the course of the movement. The initial factor analysis led us to 3 factors:

- A **link** factor, inherent in the model and accounting for part of the propagation effects on the signal. This factor is *fixed* in the experiment design sense, meaning that we have a finite number of links to consider, and control over the links used in the experiment
- A **sensor** factor, which is rather a sensor *couple* factor. As we study the difference between the sampled link qualities at each node, it is simpler in this particular case to consider sensors as a couple and study the offset generated by these sensors. This effect is also fixed
- A **passage** factor, where the same movement is repeated in the same conditions. This effect is *random*, in the sense that by actually doing the movement we randomly "pick" a particular realization of the passage from the virtual set of passages one could have done in the same conditions.

We considered a subset of links by rotating the sensors on the hands, torso and hip positions as shown on Figure 19, leading to 6 levels for both the sensor couples and the link factors, and 24 possible sensor distributions. For each sensor distribution on the body, we repeated the walk cycle 3 times. This led to a so-called *nested factorial* experiment, where the passages are hierarchically dependent on the sensors positions. A schematic view of the factorial dependency is shown on Figure 25.

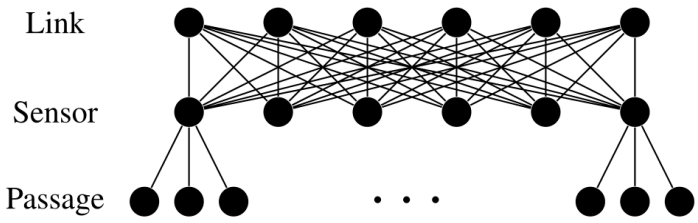

Figure 25 : Schematic representation of the experiment

The relative effects of each factor may then be extracted through classical Analysis of Variance techniques, whose results for this particular experiment design are shown below. As expected, both the link and sensor factors have a statistically significant impact on the offset, but not the repetitions of the walk cycles. The relative values of the statistics may lead one to infer that sensors have a *higher* impact than the links, but such a conclusion can only be reached through a careful analysis of the interaction between the link and sensor effects – which is significant in its own right. Since this analysis is beyond the scope of this document, the interested reader is referred to [19].

Effet	SS	d.f.	MS	F	p
Links	4515	5	902.81	590.34	$< 10^{-50}$
Sensors	166244.9	5	33248.98	21740.29	$< 10^{-50}$
Links × Sensors	11836.3	25	473.45	57.96	$< 10^{-50}$
Passage(L,S)	1120.3	72	15.56	1.37	0.09
Error	732596.7	479409	1.53		
Total	920779.2	479516			

Table 1 : ANOVA results for the experiment. (SS: Sum of Squares, d.f.: degrees of freedom, MS: Mean Square, F: Fisher-F statistic, p: p-value of the F statistic)

The results of the ANOVA are reported on Table 1[1] [22]. Since the passage effect does not deviate the offset significantly, and considering that several hours were needed to gather the whole data, we can reasonably assume that time does not affect the offset either. The conclusion is that there is indeed a significant offset in symmetry on the links as measured by the sensors, but that this *asymmetry* is stable in time and mainly dependent on the link/sensor couples considered. In a realistic WBAN, the sensors have a fixed position on the body. We can thus realistically compensate for this offset either by measuring it before the node deployment, or evaluating it *on-line* through link quality information exchange in a cooperative protocol.

4.4. OUTPUTS FOR THE PROJECT

The On-Body channel analysis of presented in this section leads to conclusions that can have a significant impact on the design of complete, cross-layer communication stacks for WBAN. This is especially true for MAC layers that will rely on channel side information for their operation.

The symmetry of the links and the temporal stability of the channel are common hypotheses made by MAC designers to propagate channel side information and optimize the parameters of the MAC layer. In a cooperative environment, these parameters may include partner selection and power allocations on the whole network. Meshed measurements in that light give a stable foundation for analysis – as shown here for the link symmetry.

Knowledge of the characteristics of the space-time correlation properties is very useful for the system optimization. More precisely, it allows a suitable choice of the relaying nodes in function of the mobility scenarios. The analysis made in section 4.2 is the same than those given in [17] and [19]. Nevertheless, the measurements were performed in the case the human subjects walked very regularly on straight line (soldier-like). Would the space-time correlation be also stationary for random walks? Deeper on-body channel correlation analysis will be presented in the D2.4 with a model.

[1] More information on how to read ANOVA tables beyond the short analysis presented here may be found in the excellent textbook ***Fundamental Concepts on the Design of Experiments***, by Hicks and Turner.

5. HUMAN ACTIVITY MONITORING MEASUREMENTS

This section describes a previous UR1 measurement campaign which has been performed in order to characterize the large scale human mobility in a real office indoor environment. The idea was to monitor over a long time period a static channel in a corridor where a regular human activity takes place and to observe what is happening and what can be deduced and applied in further indoor dynamic WBAN simulation in the physical simulator PyLayers [23]. The purpose of this measurement campaign is to identify the most important parameters related to human mobility. In the following we present a description of the measurement setup, then a mathematical formalization of the main quantities which have been post-processed and extracted from the raw measured data. The last section presents the preliminary results and illustrates how those data shade light on some quantitative aspects of the human mobility in an office corridor. The data analysis is not fully finished and the statistical modeling part is ongoing.

5.1. MEASUREMENT SETUP

An Agilent Vector Network Analyzer (E5071C) was used for the measurement. The test bed was based on a SIMO sounder (here used in SISO mode for faster acquisition time) which operates in the frequency band [1.8 - 2.2] GHz. The Tx antenna was a directive Vivaldi antenna and the Rx antenna was the central element of the antenna array shown in Figure 27 and Figure 28 respectively. A 49 meters cable was used to connect the VNA to the Tx antenna. This cable was composed of 3 connected shorter cables. The effect of those cables was calibrated off. Figure 29 shows the floor plan of the first floor of Bat 11D of the Beaulieu campus where the measurements have been made. The position of the transmitter and that of the receiver are indicated at both extremity of the corridor. The measured distance between Tx and Rx was 44.1 meters.

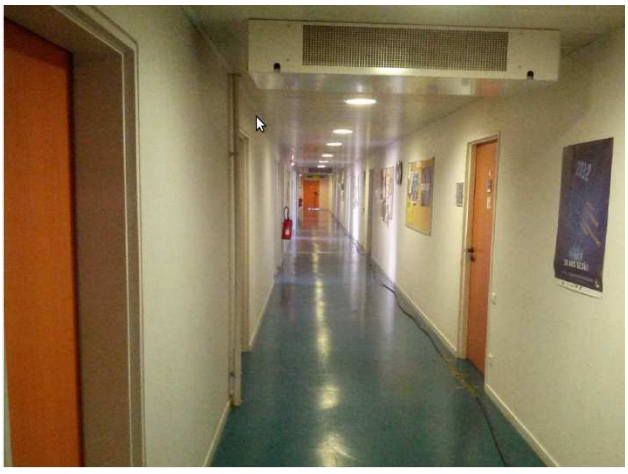

Figure 26 : The long corridor where the radio channel was regularly measured- The cable appears on the floor along the right wall Tx antenna is in front, Rx antenna is on the back.

Figure 27 : The Tx antenna on site - notice the hard fixation on the ground to avoid undesirable displacement by moving people

Figure 28 : Rx antenna is the 5th element from the left

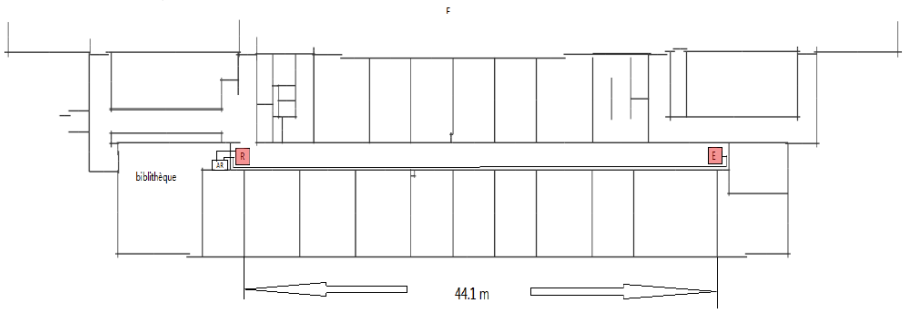

Figure 29 : Floor plan of the corridor - The measured Tx-Rx distance is 44.1meters

5.2. MATHEMATICAL FORMULATION

5.2.1 THE UNDERLYING STATIC CHANNEL

Let us define $\bar{h}(\tau)$ the static SISO channel impulse response. The frequency domain counterpart is the static channel transfer function obtained after a Fourier transform:

$$\bar{H}(f) = \mathcal{F}_{\tau}\{\bar{h}(\tau)\} \tag{10}$$

Those two quantities are here assumed perfectly static and do not depend on time. In the following we are interested in the observed deviation from those idealistic quantities.

5.2.2 MEASURED RAW DATA $S_{21}(f,t)$

In practice the network analyzer gives access to a realization of the actual channel transfer function with a high dynamic range. The measured quantity is varying from one acquisition to another for three main reasons: the additive noise, the additive interference and the channel dynamics, mostly caused by human activity taking place into the propagation environment.

This can be modeled as the sum of the three different above mentioned sources of received power:

$$S(f,t) = \bar{H}(f) + \delta H(f,t) + I(f,t) + N(f,t) \tag{11}$$

Here t denotes the time of acquisition which, in the present study, is several hours. In a practical system, the channel acquisition is made with a uniform sampling rate, the time is then discretized as $t_k = t_0 + k\delta_t$ and δ_t denotes the sampling rate. In this particular study the values of δ_t are 30s for measurement run 1 and 10s for measurement run 2. $N(f,t)$ and $I(f,t)$ denote respectively the noise and interference contribution to the measured channel transfer function.

The measured data are regularly sampled, the discretized transfer function is then more properly represented with a discretized notation as:

$$S(f,k) = \bar{H}(f) + \delta H(f,t) + I(f,k) + N(f,k) \tag{12}$$

As the behaviour of the channel over a long time period is not stationnary, it is necessary to observe the channel during a steady period in order to construct a good estimate of the static transfer function. The averaged channel transfer function over K realizations is given by

$$\mu_K(S(f,k)) = \bar{H}(f) + \mu_K(\delta H(f,k)) + \mu_K(I(f,k) + N(f,k)) \tag{13}$$

Or equivalently

$$\mu_K\big(S(f,k)\big) = \bar{H}(f) + \mu_K\big(\delta H(f,k)\big) + \varepsilon_K(f,k) \tag{14}$$

As the averaging is taken on a steady period, the perturbation is assumed being negligible

$$\mu_K^{steady}\big(S(f,k)\big) \approx \bar{H}(f) + \varepsilon_K(f,k) \tag{15}$$

with

$$\varepsilon_K(f,k) = \mu_K(I(f,k) + N(f,k)) \tag{16}$$

The interference is not uniformly distributed neither in the frequency nor in the time domain.

At that point, for the other portion of the acquisition where human perturnation is observed we define the delta-K Channel Transfer Function (DCTF) as the difference between each realization and the previously determined K-averaged steady channel transfer function.

$$\delta_K S(f,k) = S(f,k) - \mu_K^{steady}\big(S(f,k)\big)$$

$$\delta_K S(f,k) = \delta H(f,k) + \varepsilon(f,k) - \varepsilon_K(f,k)$$

$$\delta_K S(f,k) = \delta H(f,k) + \varepsilon_K^c(f,k) \tag{17}$$

Notice that the static channel transfer function $\bar{H}(f)$ is removed from this quantity.
The new term only contains the pertubation of the channel plus a centered noise term which includes narrow band interferences and measurement noise.

The human motion is more meaningfuly visible in the time domain as the moving bodies are selectively crossing different specular contributions of the radio channel. So, let's apply an inverse Fourier transform along the frequency axis to get a time/delay representation of the perturbated channel.

$$\delta_K s(\tau,k) = \mathcal{F}^{-1}\{\delta H(f,k) + \varepsilon_K^c(f,k)\}$$

$$\delta_K s(\tau,k) = \delta h(\tau,k) + \varepsilon_K^c(\tau,k) \tag{18}$$

$\delta_K s(\tau,k)$ is a complex quantity which is a function of delay and which brings an information on which portions of the channel impulse response are the more varying due to human perturbation of the channel plus a perturbating term due to interference which can be large from time to time. The phase term should be informative but has not been exploited yet. This

is likely that in most of the situations, Tx and Rx are in a line of sight (LOS) condition. When the LOS path is interrupted, by a body for instance, high variance on the LOS contribution appears. A very interesting part is on the variability of weak paths. As we will see below the time integration allows to detect very weak amount of variation and is very sensitive. The empirical variance over a time window of length L of the above quantity is a pure function of delay and is defined as.

$$v_L(\tau) = \mu_L(\delta_K s(\tau,k)\,\delta_K^* s(\tau,k)) \tag{19}$$

Those time window will be defined to correspond to meaningful portion of time as for example a full day. Very interestingly, it would be shown below that those variance profiles are very similar from time to time and that the scaling factor between two realizations can be proposed to quantify the amount of human mobility during a day.

5.3. PRELIMINARY RESULTS

The first run goes from April 18th 2013 at 14:30 until April 19th 2013 at 17:30. This corresponds to 3240 aggregated transfer functions (3240 x 30 = 97170 seconds = 1620 minutes = 27 hours). The second run goes from Thursday April 19th 2013 15:30 to Tuesday 23 at 13:30, this corresponds to 333000 aggregated channel transfer functions.

The raw data S21 as a function of acquisition time are shown in Figure 30 for run 1 and the module of difference with mean value in Figure 31 for run 2. Strong variations due to the human activity are clearly visible in both run for working day period. The long term structure of the interference is also clearly visible in Figure 31

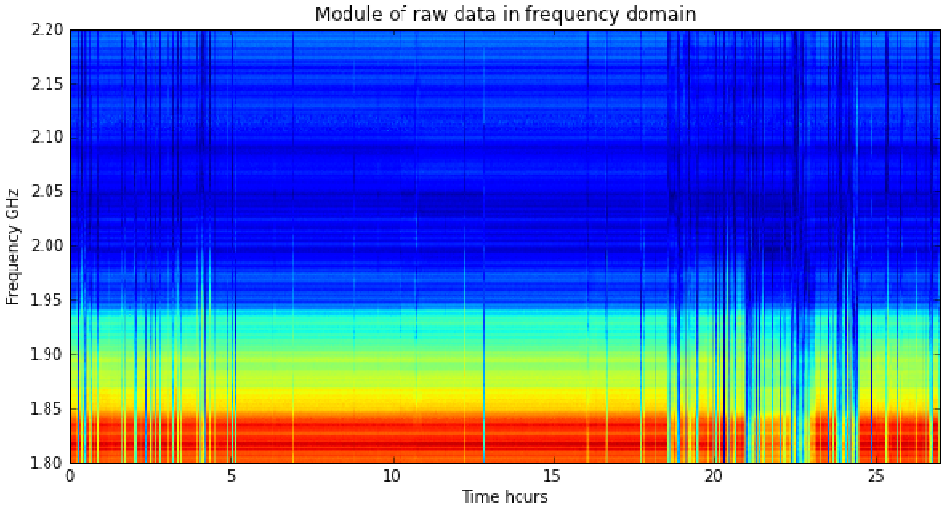

Figure 30 : $S_{21}(f,t)$ for the first run Thursday April 18th 14:30 to Friday April 19th 17:30

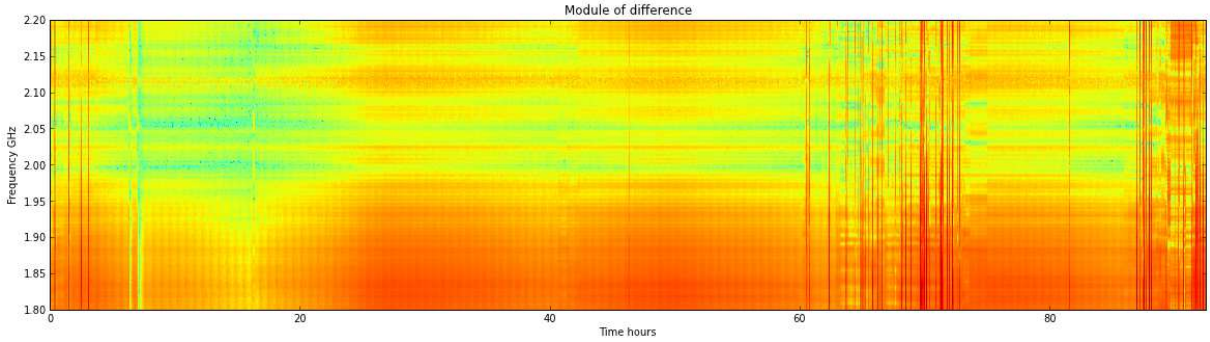

Figure 31 : Module of difference of Channel transfer function over 90 hours April 19th to April 23th

The following four figures illustrate the $\delta_K s(\tau, k)$ for different time period and K=100.

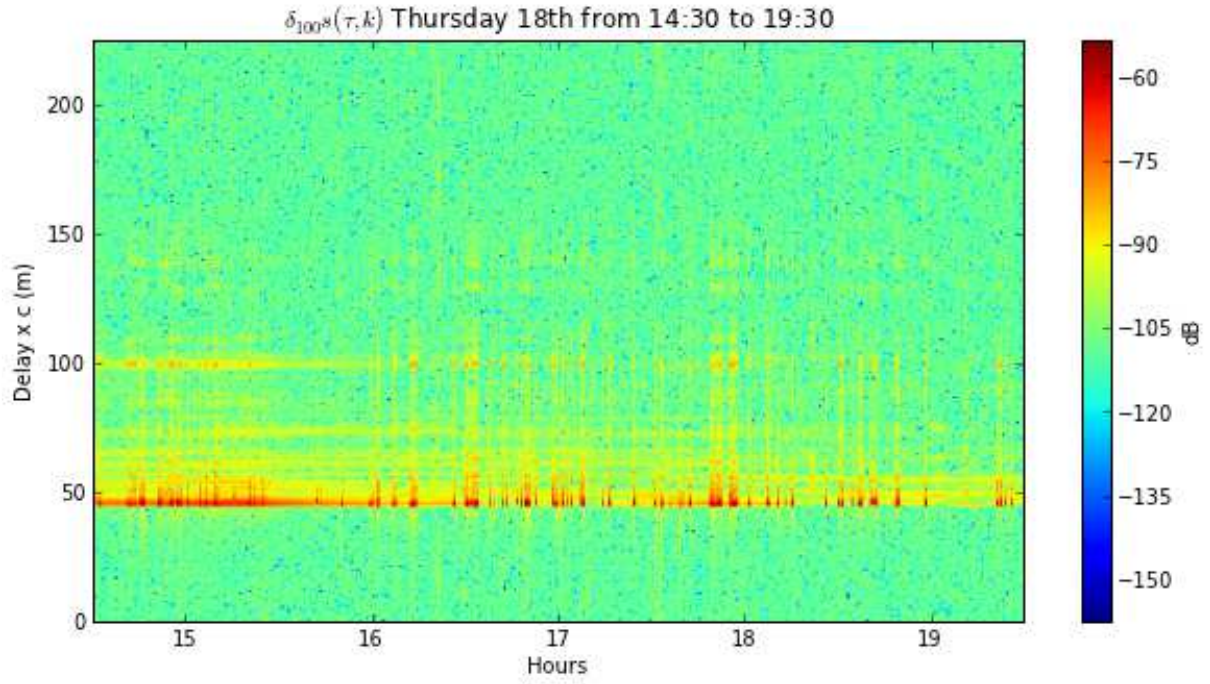

Figure 32 : Run1 delta channel impulse response as a function of time (ts=30s) April 18th from 14:30 pm to 19:30 pm – Normal working office day activity in the afternoon.

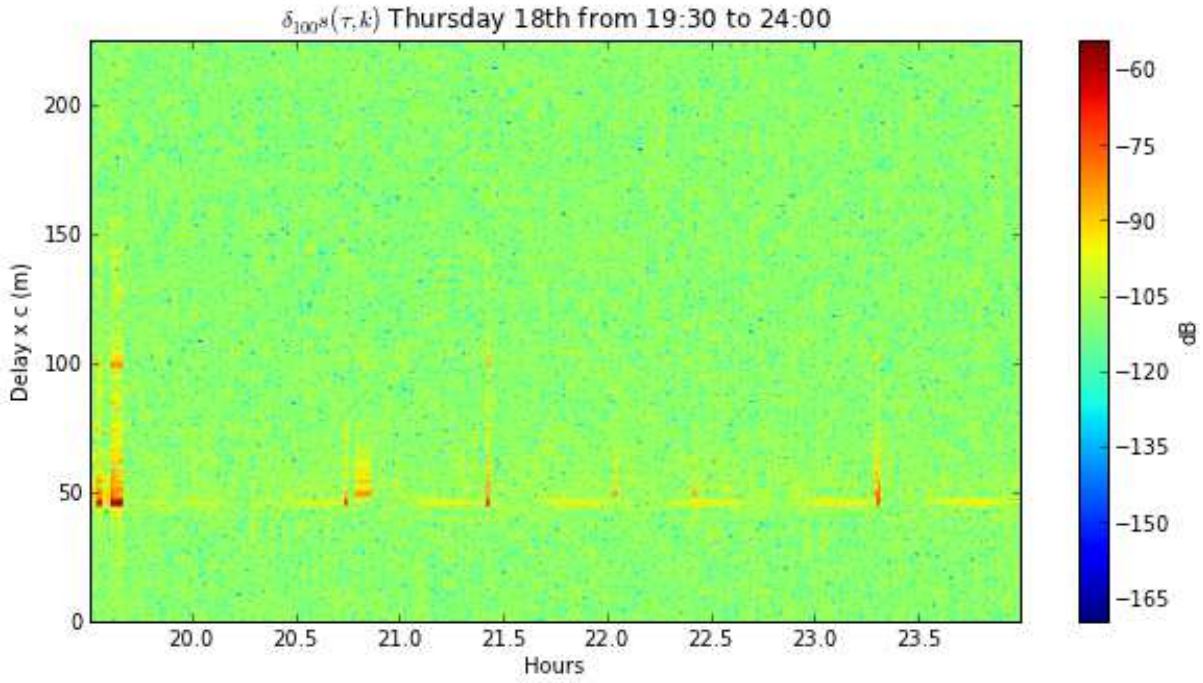

Figure 33 : Run1 delta channel impulse response as a function of time (ts=30s) April 18th from 19:30 pm to 24:00am – evening activity sporadic channel perturbation

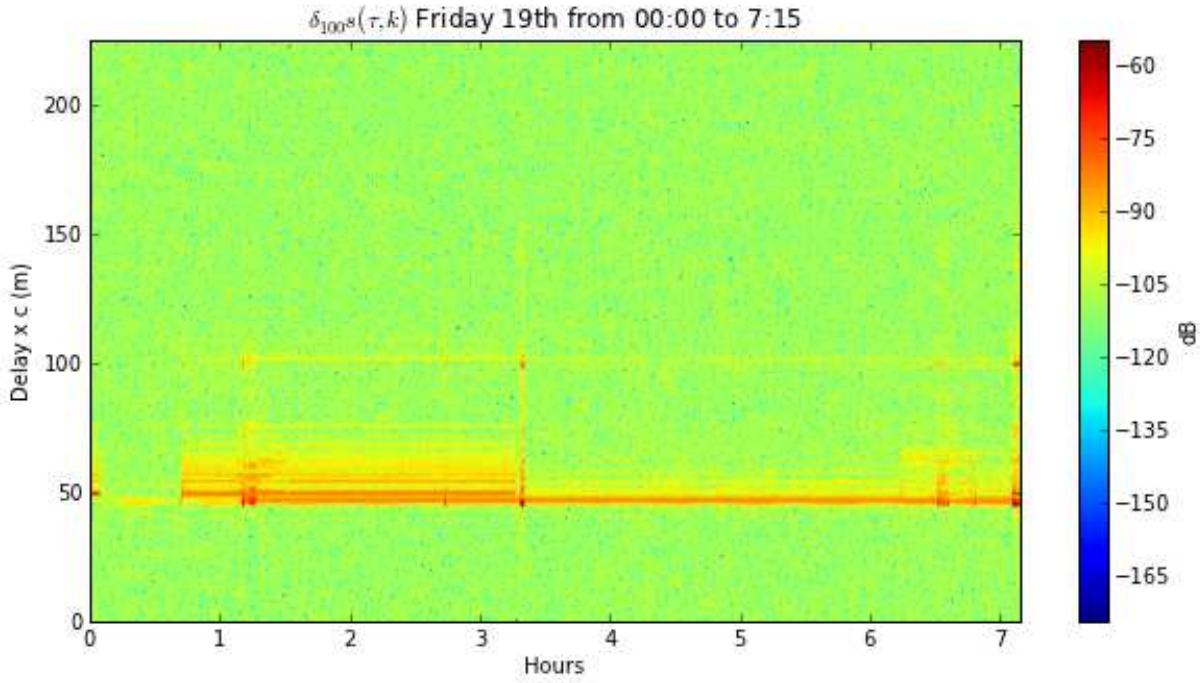

Figure 34 : Run1 delta channel impulse response as a function of time (ts=30s) April 18th from 00:00 to 7:15 – Nocturn activity, channel has been modified permanently from 00:40 to 3:20 + early morning activity.

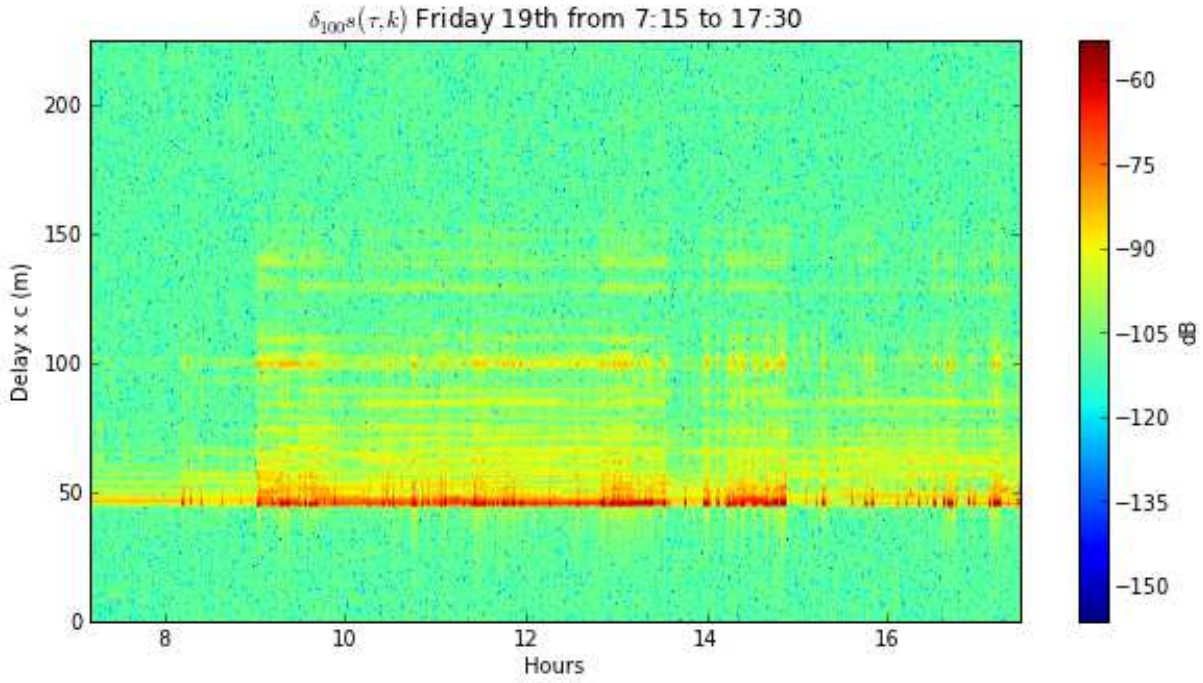

Figure 35 : Run1 delta channel impulse response as a function of time (ts=30s) April 19th from 7:15 to 17:30 – Normal working office day activity in the morning and in the afternoon

Figure 36 represents on a same plot the static channel impulse response, the mean value of the variation around the static channel and the variance of this variation calculated over the whole duration of the selected portion of the signal which goes from April 18th from 14:30 to 19:30. Interestingly the variance curve provides information about weak paths which have large variability. This could be interpreted by the fact that with respect to the human motion taking place in the corridor, there exist paths which late time of arrival can be strongly affected. The variance of the channel given as a function of the delay depends both on the channel itself and on its relation with the human mobility pattern. This human mobility pattern is almost the same shape from one period to another as illustrated on Figure 37. Figure 37 represents the variance for the 4 considered period of time extracted from the 25 hours of run 1 acquisition. Day and night have clearly different pattern. The integral of those functions could be interpreted as an intensity of activity (meaning independent of the actual period of observed time). Blue curve and cyan curve correspond to day working activity, and green and red correspond to night activity.

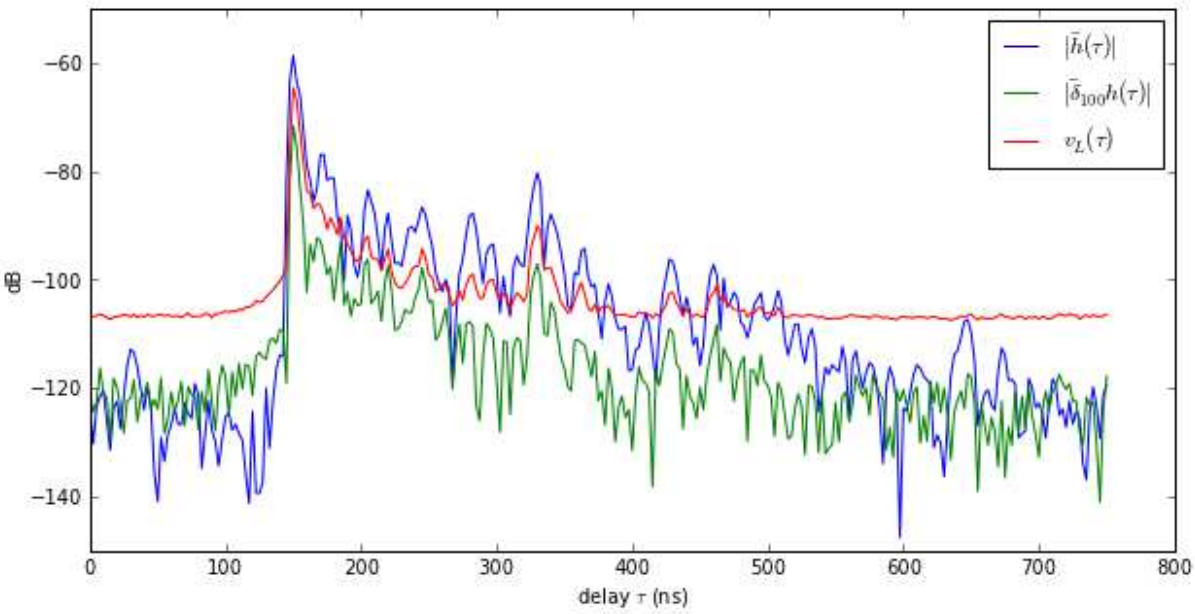

Figure 36 : static channel impulse response (blue), mean delta perturbation (green), variance of the delta perturbation (red). April 18th from 14 :30 to 19:30 – Normal working office day activity in the afternoon.

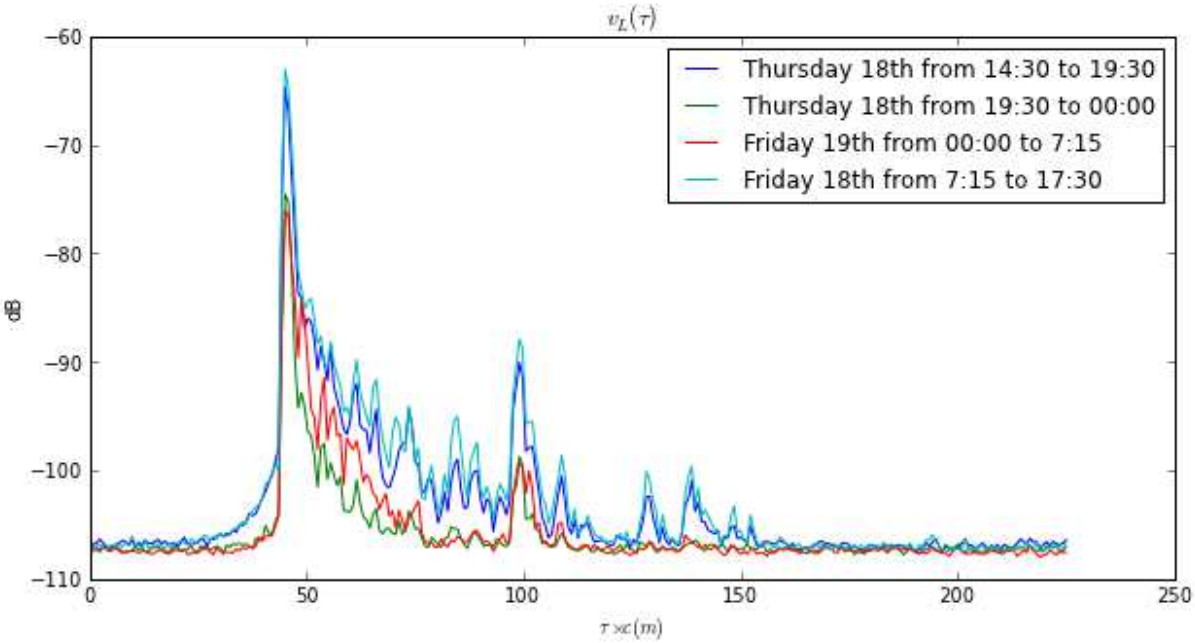

Figure 37 : Variance of the channel variation due to human activity obtained for the different chosen period of time.

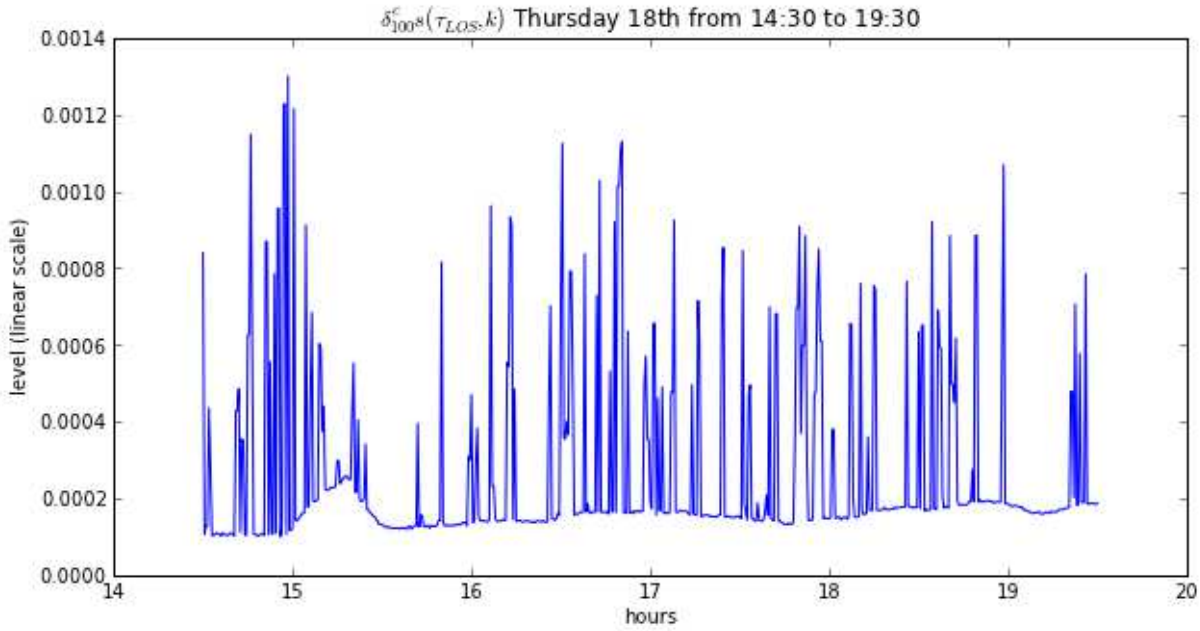

Figure 38 : variation around LOS path as a function of time. (ts=30s) April 18th from 14:30 to 19:30

Figure 38 represents the variation around the LOS during a day with normal office activity in the afternoon from April 18th from 14:30 to 19:30. The interference level is not constant. This is the kind of data which is currently exploited to provide an indication of the quantitative variation of the Poisson process parameter which drives the punctual process. This information will be summarized into a corridor building human activity and a similar behavior will be reproduced in simulation. For example Figure 40 gives the real variation observed on the LOS path as well as the corresponding moving average with a sliding window of 1 hour. In particular we are considering two Poisson processes in order to model the beginning and the end of the perturbation. We have observed that the perturbation of the channel has a variable duration which follows very well an exponential law. This work on extracting and modeling the large scale time dynamic parameters of the channel perturbation is ongoing. As a simple illustration of how those data will be exploited later in the CORMORAN in relation with other simulation tasks, Figure 40 is a simple example of how can be generated a similar punctual process. This kind of modeling will feed the state machine which handles the large scale mobility of agents in an indoor environment.

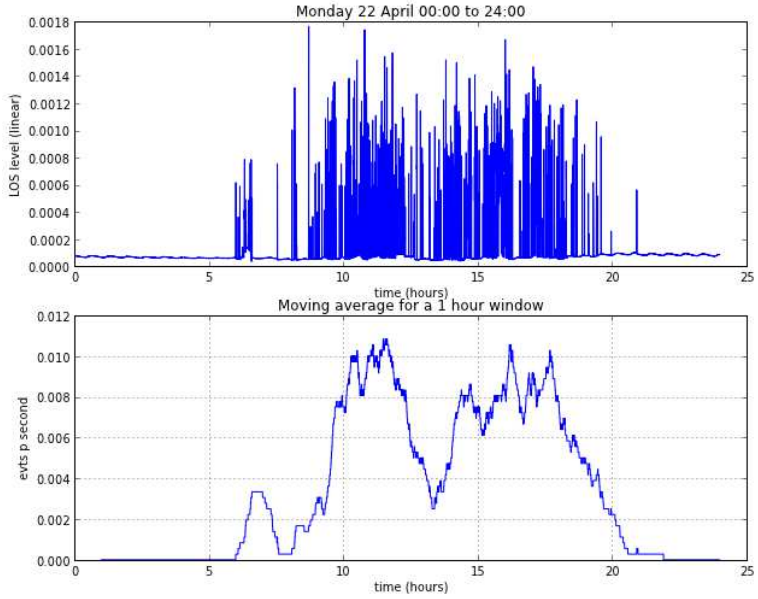

Figure 39 : Run 2 extraction of Poisson process parameter from real data

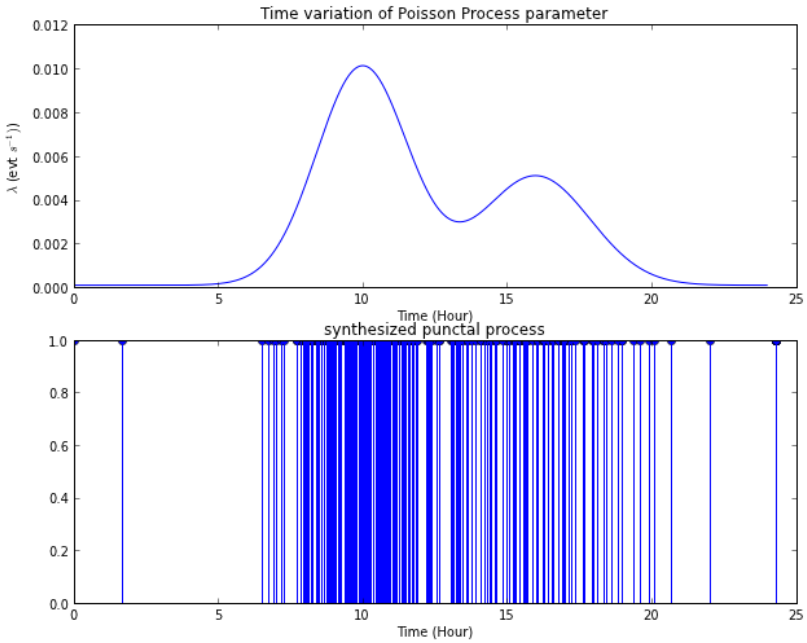

Figure 40 : Example of a simple simulated synthesized punctual Poisson process

6. CONCLUSIONS

Final data channel measurements are now available and exploitable for the sub-task ST2.3 concerning the characterization and the statistical modeling of WBAN links. Some of the measurements have already been partially processed and analyzed. For instance, preliminary processing and analysis have been carried out on *Off-body* measurements using a modeling tool presented in the D2.2. In addition to these measurements, some previous measurement campaigns have also been analyzed and characterized.

One of the objectives of the ST2.3 will be to provide a comprehensive UWB *Off-body* channel model based on the measurements presented in section 2. This model will be useful for the validation of the deterministic channel model developed by UR1, especially on the characterization of the angles of arrival. It also provides useful information for the design of localization systems such as the time of arrival of the strongest multi-path component.
A space-time correlation model will also be provided in the cooperative communication context in which the measurements presented in section 3 have been presented. This model will be completed by the analysis of previous *On-body* CEA measurements performed in various walking scenarios.
Finally, the characterization of the previous UR1 human mobility monitoring measurements will allow feeding the development of the physical simulator related to the sub-task ST2.4.

7. REFERENCES

[1] O. P. Pasquero, R. D'Errico, M. Mhedhbi and B. Uguen, "D2.2: 1st Channel Measurement Campaign and Identification of Relevant Radio Models and Parameters", March 2013

[2] B. Denis, J. Hamie, R. D'Errico, O. P. Pasquero, C. Goursaud, J. Guizar, A. Mauricio, P. Ferrand, J.-M. Gorce, C. Chaudet, B. Uguen, S. Avrillon and M. Mhedhbi, "D1.1: Application Scenarios, System Requirements and Prior Models", July 2012

[3] M. Mhedhbi, S. Avrillon, B. Uguen, M. Pigeon, R. D'Errico and O. P. Pasquero, "D2.1 : On-Body Antennas Characterization & Exploitable Radiation Properties", Oct. 2012

[4] E. Guéguen, F. Thudor and P. Chambelin, "A low cost UWB printed dipole antenna with high performance", in Proc. in IEEE International Conference on Ultra-Wideband (ICU), 2005

[5] R. Rosini and R. D'Errico, "Comparing On-Body Dynamic Channels for Two Antenna Designs", in *Antennas and Propagation Conference (LAPC),* 2012 Loughborough, pp. 1-4

[6] B. H. Fleury, D. Dahlaus, R. Heddergott, and M. Tschudin, "Wideband Angle of Arrival Estimation using the SAGE Algorithm", International Symposium on Spread Spectrum Techniques and Applications, ISSSTA 1996

[7] B. H. Fleury, M. Tschudin, R. Heddergott, D. Dahlaus, K. I. Pedersen, "Channel Parameter Estimation in Mobile Radio Environments Using the SAGE Algorithm", Journal on Selected Areas in Communications, vol. 17, no. 3, March 1999

[8] A. P. Dempster, N. M. Laird, and D. B. Rubin, "Maximum likelihood from incomplete data via the EM algorithm," J. Royal Statist. SOc., Ser. B, vol. 39, no. 1, PP. 1-38, 1977

[9] C. Chong, D. I. Laurenson, C. Tan, S. McLaughlin, M. A. Beach, and A. Nix, "Joint detection-estimation of directional channel parameters using the SAGE algorithm", IEEE International Conference on Communications, vol. 2, New York, USA, April 2002, pp. 906-910

[10] M. Matthaiou and N. Nrazavi-Ghods, "Characterization of an indoor MIMO channel in frequency domain using the 3D-SAGE algorithm", in IEEE International Conference on Communications, vol. 24-28, June 2007, pp. 5868 – 5872

[11] K. Haneda and J.-I. Takada, "An application of SAGE algorithm for UWB propagation channel estimation", in IEEE Conference on Ultra Wideband Systems and Technologies, Nov. 2003, pp. 483 – 487

[12] K. Haneda, J.-I. Takada, and T. Kobayashi, "Experimental evaluation of a SAGE algorithm for ultra wideband channel sounding in an anechoic chamber," in International Workshop on Joint UWBST & IWUWBS, May 2004, pp.66-70

[13] S. V. Roy, C. Oestges, F. Horlin and Ph. De Doncker: On-body propagation velocity estimation using ultra-wideband frequency-domain spatial correlation analysis, El. Letters, vol. 43, n° 25, Dec. 2007

[14] A. Richter, J. Salmi and V. Koivunen, "An Algorithm for Estimation and Tracking of Distributed Diffuse Scattering in Mobile Radio Channels", *in Proc. of IEEE 7th International Workshop on Signal Processing Advances for Wireless Communications*, Jul. 2006

[15] F. Quitin, C. Oestges, F. Horlin and P. De Doncker, "A Polarized Clustered Channel Model for Indoor Multiantenna Systems at 3.6 GHz", *IEEE Trans. On Vehicular Technology*, Oct. 2010

[16] O. P. Pasquero, R. Rosini, R. D'Errico and C. Oestges, "On-Body Channel Correlation in Various Walking Scenarios", IC 1004 COST, May 2013

[17] R. D'Errico and L. Ouvry, "A Statistical Model for On-Body Dynamic Channels", *International Journal of Wireless Information Networks*, vol. 17, pp. 92-104, 2010, Available: http://dx.doi.org/10.1007/s10776-010-0122-0

[18] S. van Roy, F. Quitin, L. Liu, C. Oestges, F. Horlin, J. Dricot and P. De Doncker, "Dynamic Channel Modeling for Multi-Sensor Body Area Networks", *Antennas and Propagation, IEEE Transactions on,* vol. 61, no. 4, pp. 2200-2208, 2013

[19] M. Lauzier, P. Ferrant, A. Fraboulet, H. Parvery and J.-M. Gorce, "Full Mesh Channel Measurements on Body Area Networks under Walkinf Scenarios", *in Proc. European Conf. on Antennas and Propagation,* 2013

[20] P. Ferrand, C. Goursaud and J.-M. Gorce, "On the packet error rate of correlated shadowing links in Body Area Networks", *in Proc. Eur. Conf. on Antennas and Propagation (EUCAP),* 2011

[21] K. Y. Yazdandoost and K. Sayrafian-Pou, "*Channel Model for Body Area Networks (BAN) IEEE 802.15.6 Body Area Netwrks Workgroup*", Technical Report, 2009

[22] C. Hicks and K. Turner, "*Fundamental Concepts in the Design of Experiments*", Oxford University Press, 1999

[23] http://pylayers.github.io/pylayers/